Bile acids target an exposed cavity in the glucocorticoid receptor modulating receptor self-assembly, chromatin binding and transcriptional activity

Alba Jiménez-Panizo[1,2,3], Thomas A. Johnson[2], Kaustubh Wagh[2], Andrea Alegre-Martí[1], Inés Montoya Novoa[1], Agustina L. Lafuente[4], Ulrich Eckhard[5], Luis Ángel Rodríguez-Lumbreras[3], Le Hoang[2], Martín Stortz[2,6], Montserrat Abella[1], Ido Goldstein[7], Annabel Valledor-Fernández[1], Lyuba Varticovski[2], Irwin Arias[8], Diego M. Presman[4], Diana A. Stavreva[2], Juan Fernández-Recio[3], Pablo Fuentes-Prior[1]*, Gordon L. Hager[2]*, Eva Estébanez-Perpiñá[1]*

Affiliations

[1] Department of Biochemistry and Molecular Biomedicine, Faculty of Biology, University of Barcelona (UB). Institute of Biomedicine of the University of Barcelona (IBUB), University of Barcelona (UB), 08028 Barcelona, Spain

[2] National Cancer Institute, National Institutes of Health, Bethesda, MD 20892-5055, USA

[3] Instituto de Ciencias de la Vid y del Vino (ICVV), CSIC - Universidad de La Rioja – Gobierno de La Rioja, 26007 Logroño, Spain

[4] IFIBYNE, UBA-CONICET, Universidad de Buenos Aires, Facultad de Ciencias Exactas y Naturales, Buenos Aires, C1428EGA, Argentina.

[5] Department of Structural and Molecular Biology, Molecular Biology Institute of Barcelona (IBMB-CSIC), 08028 Barcelona, Spain.

[6] Instituto de Química Biológica de la Facultad de Ciencias Exactas y Naturales (IQUIBICEN), CONICET-Universidad de Buenos Aires, Buenos Aires C1428EGA, Argentina.

22   [7] Institute of Biochemistry, Food Science and Nutrition, The Robert H. Smith Faculty of

23   Agriculture, Food and Environment, The Hebrew University of Jerusalem, POB 12, Rehovot

24   7610001, Israel.

25   [8] Office of the Director, National Institutes of Health, Bethesda, MD 20892-5055, USA

Corresponding authors

*These authors jointly supervised this work.

- Eva Estébanez-Perpiñá. E-mail: evaestebanez@ub.edu

- Gordon L. Hager. E-mail: hagerg@dce41.nci.nih.gov

- Pablo Fuentes-Prior. E-mail: fuentespriorpablo@gmail.com

Abbreviations

37	AF	Activation function
38	AR	Androgen receptor
39	BF-3	Binding function-3
40	BOG	octyl beta-D-glucopyranoside
41	CA	Cholic acid
42	CDCA	Chenodeoxycholic acid
43	CHAPS	3-[(3-cholamidopropyl) dimethylammonio]-1-propanesulfonate
44	Cort	Corticosterone
45	DCA	Deoxycholic acid
46	Dex	Dexamethasone
47	ER	Estrogen receptor
48	E site	Entry/exit site
49	FXR	Farnesoid X receptor
50	GC	Glucocorticoid
51	GR	Glucocorticoid receptor
52	LBD	Ligand-binding domain
53	LBP	Ligand-binding pocket
54	LCA	Lithocholic acid
55	MR	Mineralocorticoid receptor
56	N&B	Number and brightness
57	PDB	Protein Data Bank
58	PR	Progesterone receptor
59	RNA-seq	RNA sequencing
60	SF-3	Sensor function-3
61	SMT	Single-molecule tracking
62	SPR	Surface plasmon resonance
63	TauroCA	Taurocholic acid
64	TauroUDCA	Tauroursodeoxycholic acid
65	UDCA	Ursodeoxycholic acid
66	VdW	Van der Waals
67	WT	Wild type

68

Abstract

The glucocorticoid receptor (GR) is an essential transcription factor that controls metabolism and homeostasis. Glucocorticoids (GCs) activate the GR upon occupying the internal ligand-binding pocket (LBP) of its ligand-binding domain (GR-LBD), which has been the focus of most previous structure-function studies. Synthetic GCs such as dexamethasone are widely used to treat inflammatory diseases, but their chronic use results in major side effects, whose molecular underpinnings remain unresolved. Here we present a thorough analysis of the topography of GR-LBD and its ability to bind small-molecule compounds, especially cholesterol derivatives. We show that one important class of steroids, bile acids, bind to previously unidentified and highly conserved, surface-exposed cavities on GR-LBD. We show that bile acids affect GR turnover and self-assembly in living cells, modulating receptor transcriptional activity. These findings reveal a previously unrecognized mechanism of GR regulation, with implications for the design of GCs with novel mechanisms of action.

82   **Teaser**

83   Bile acids modulate the activity of the glucocorticoid receptor upon binding to an exposed

84   allosteric pocket thereby influencing transcriptional regulation and receptor self-assembly in

85   living cells.

INTRODUCTION

Nuclear receptors (NRs) tightly control a large spectrum of biological processes such as cell proliferation, metabolism, and homeostasis[1–3]; and are therefore one of the major pharmaceutical targets for many conditions including various cancer types, as well as inflammatory and metabolic diseases[4–9]. Because of their extraordinary pharmacological relevance, structure-function investigations of NRs have almost exclusively focused on their hormone- or ligand-binding pockets (LBPs), internal cavities within the ligand-binding domains (LBDs) mostly lined by aliphatic/aromatic residues[10–13]. However, evidence accumulated over the last two decades indicates the presence of surface-exposed pockets in several nuclear receptors that accommodate small molecules including endogenous hormones, metabolic compounds, and pharmacologically active molecules[14–18].

Steroid receptors are a subfamily of NRs that bind with high affinity to a plethora of cholesterol-derived molecules collectively known as steroids[19]. The subclass includes the closely related receptors for glucocorticoids (GR; termed NR3C1 in the systematic nomenclature) and mineralocorticoids (MR; NR3C2), together with four members that control physiological processes of the reproductive system: the androgen receptor (AR; NR3C4), the progesterone receptor (PR; NR3C3), and estrogen receptors α (ERα; NR3A1) and β (ERβ; NR3A2)[1].

The binding of pharmacologically relevant small-molecule compounds outside the LBP was first described for estrogen receptors[14,20]. The crystal structure of ERβ-LBD bound to 4-hydroxy-tamoxifen, the most abundant active tamoxifen metabolite, revealed the inhibitor occupying not only the LBP but also a surface groove that represents the major binding site of NR coregulators, also known as activating function 2 (AF-2)[20–24]. This feature may account for the mixed agonist/antagonist activity of type I antiestrogens such as tamoxifen and might explain its extraordinary success in the treatment of ER-positive breast cancer (recently reviewed in ref. [25]).

110   Nonsteroidal anti-inflammatory drugs and thyroid hormones that bind the AF-2 of AR have been

111   identified as potential antiandrogens[16]. Finally, the AF-2 clefts of receptors from other subfamilies

112   such as the thyroid hormone receptor α (TRα; NR1A1)[15] and the vitamin D receptor (VDR;

113   NR1I1)[17] are also targeted by small molecules.

114   In addition to AF-2, we have previously identified a contiguous, solvent-exposed surface

115   on AR-LBD that binds multiring compounds including thyroid hormones, called binding function

116   3 (BF-3)[16]. Of particular note, the AR BF-3 is a docking site for chaperones and co-chaperones[16,26–

117   28]. Binding of a non-steroidal ligand to BF-3 inhibited AR by preventing its hormone-dependent

118   dissociation from the Hsp90:FKBP52 complex[26]. This site is also conserved across NR subfamilies

119   and suitable for drug intervention[16,29]. For instance, BF-3 regulates interactions with the linker

120   between the DNA-binding domain and LBD of HNF4α (NR2A1)[30]. Finally, small-molecule

121   compounds that bind outside the LBP have been reported in other receptor subfamilies, most

122   notably for TRα[15,31] and Nur77 (NR4A1)[32], highlighting alternative modes of receptor modulation

123   beyond the conventional ligand-binding paradigm. Despite substantial evidence indicating that

124   well-defined surface cavities on the LBDs of nuclear receptors serve as functional binding sites

125   with high druggability potential[18], a thorough and systematic exploration of their structural

126   topography remains limited. Moreover, co-crystal structures have remained an underutilized

127   resource in drug discovery, with their valuable insights often overlooked in the search for new

128   mechanisms of action and novel therapeutic targets.

129   Bile acids are a class of endogenous cholesterol-derived steroidal molecules that play

130   essential physiological roles in nutrient absorption[33–35], metabolism[36–39], autophagy[40] and

131   longevity[41]. In addition to their well-characterized, non-specific activities as emulsifiers, bile acids

132   are gaining increased attention as important signaling molecules in physiological pathways

133   including hepatic lipid and energy metabolism, inflammation and immune homeostasis[42–44], with

134   important implications for disease[45–52]. These signaling activities of bile acids are mediated, at

135   least partially, through their specific LBP-mediated interaction with farnesoid X receptor (FXR;

136   NR1H4) together with liver X receptors α and β (LXRα; NR1H3 and LXRβ; NR1H2,

137   respectively)[53–59], as well as NR1I receptors, VDR[17,60,61], pregnane X receptor (PXR; NR1I2)[62,63],

138   and constitutive androstane receptor (CAR; NR1I3)[64,65]. Accordingly, these members of the NR1H

139   and NR1I subfamilies are collectively termed bile acid-activated receptors (BARs)[44,66].

140   The gut microbiota plays a pivotal role in bile acid metabolism by converting primary into

141   secondary bile acids. Primary bile acids, such as cholic acid (CA) and chenodeoxycholic acid

142   (CDCA), are synthesized in the liver from cholesterol, conjugated with taurine or glycine, and

143   secreted into bile, from where they are released into the intestine[67–69]. Once in the intestine, gut

144   bacteria modify bile acids through enzymatic processes such as deconjugation and

145   dihydroxylation[39,70,71]. These microbial transformations are crucial for maintaining the size and

146   composition of the bile acid pool, which in turn influences hepatic and intestinal signaling

147   pathways, including those mediated by FXR[72,73]. The glucocorticoid receptor has been connected

148   to the regulation of inflammatory and immunomodulatory effects of bile acids such as

149   ursodeoxycholic acid (UDCA)[74]. In addition, GR but not FXR modulates the therapeutic potential

150   of the taurine-conjugated UDCA derivative, tauroursodeoxycholic acid (TauroUDCA), in

151   preclinical models of the neurogenerative disorder, spinocerebellar ataxia type 3[75].

152   Here we present a detailed analysis of the molecular topography of the ligand-binding

153   domains of GR and other steroid receptors compared to that of canonical BARs. We identify

154   common and unique cavities with ligand binding capabilities similar to those of the LBP and AF-

155   2 pockets. GR, in particular, features a unique cavity predominantly lined by residues from helices

156   H9/H10, which is important for receptor self-assembly and transcriptional activity *in vivo*. We

157   explore the consequences of bile acid binding to this previously uncharacterized surface pocket on

158   GR-LBD, demonstrating that it represents an actionable target for modulating both acute and long-

159   term exposure to glucocorticoids. This binding event has significant implications for the

160   glucocorticoid receptor function and offers potential avenues for therapeutic intervention.

161

162   **RESULTS**

163   **The hormone-binding domain of the glucocorticoid receptor features solvent-exposed**

164   **cavities with high ligand-binding potential and significant druggability**

165   To explore the topography of the LBD modules from GR and other steroid receptors, we conducted

166   a thorough bioinformatics analysis using state-of-the-art programs for pocket detection and

167   druggability potential[76–78]. For comparison, we also analyzed the LBDs of two BARs, FXR and

168   VDR, for which structural evidence of bile acid binding has been reported[17,58,60]. The results of

169   these analyses are presented in Fig. 1A, Fig. S1A and Tables S1 to S3. As expected, the well-

170   characterized LBP and AF-2 pockets of all receptors are identified with high ligand-binding

171   abilities and medium to strong druggability. However, we observed large differences regarding

172   other surface cavities. Most notably, all programs consistently identify a major cavity in the GR-

173   LBD surface lined by residues from helices H9/H10 and the connecting loop, L9-10, with a higher

174   ligand-binding ability than the LBP and a medium druggability score (Table S1). The previously

175   characterized BF-3 site is also identified in this systematic unbiased analysis, but with weak

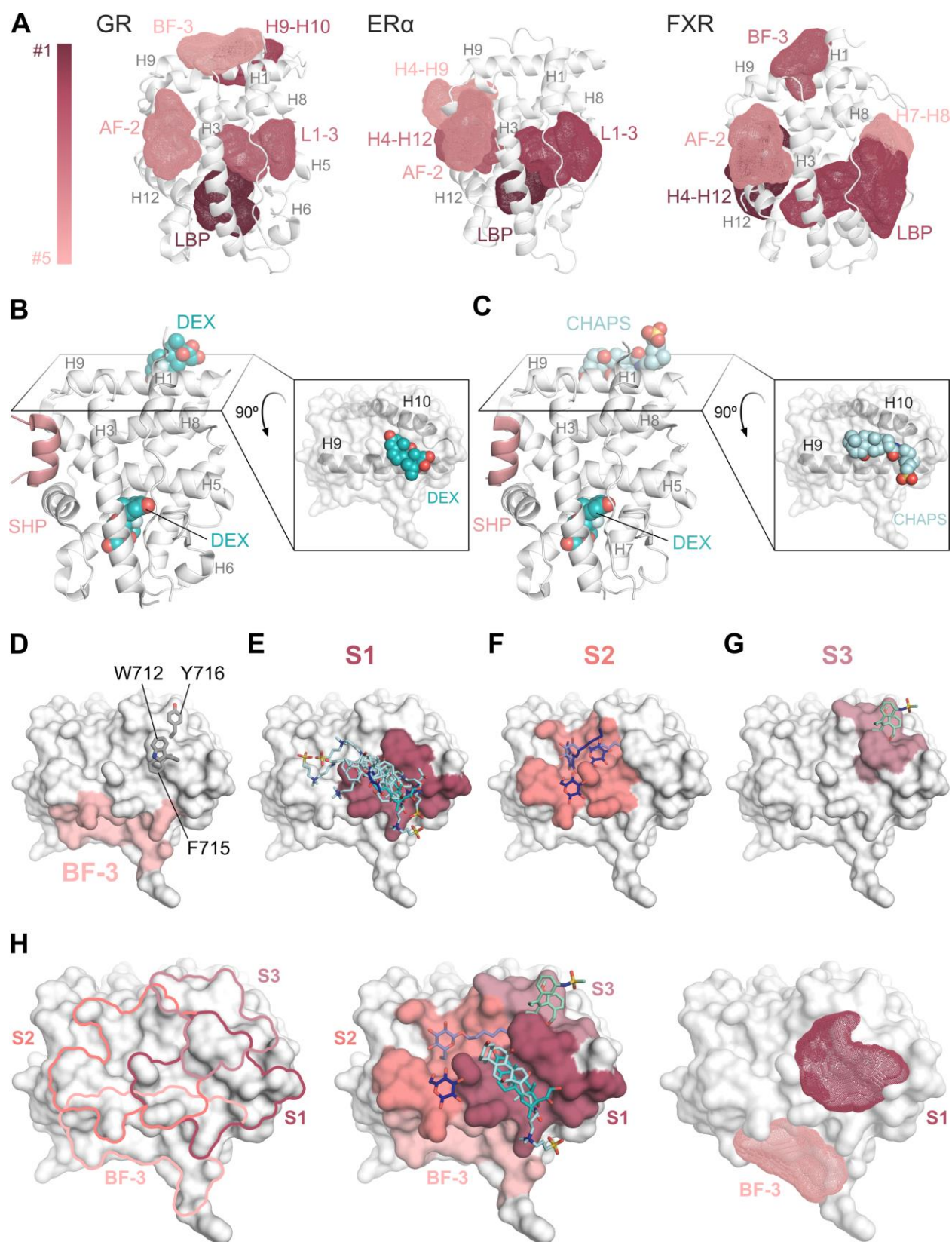176   druggability (Fig. 1A).

177

11

Fig. 1. The ligand binding domain of GR and other nuclear receptors display several well-defined solvent-exposed cavities.

Fig. 1 Legend. A, Representation of the top five cavities in the LBD of two steroid receptors, GR and ERα, as compared to FXR. Major helices and loops are labeled. Pockets are colored based on their druggability scores. Note the unique cavity network of GR-LBD. **B, C**, Small-molecule compounds such as Dex or CHAPS bind to a GR-LBD cavity formed by helices H9/H10 and the connecting loop, L9-10. GR-LBD is depicted as a white cartoon and bound small molecules are shown as color-coded sticks (PDB codes 7YXP and 7YXO, respectively). **D**, Surface representation of the GR domain viewed from the top in the standard orientation. The BF-3 site is highlighted in salmon. Aromatic residues at the N-terminus of H10 are shown as sticks and labeled. **E-G**, Superimposition of all compounds that bind at the major surface-exposed cavity of GR-LBD in deposited crystal structures. Depending on the contact residues, three different subsites can be defined. (**E**) The most frequently targeted subsite S1 includes residues from the more C-terminal end of H9, the L9-10 loop, and Trp712 / Phe715 in H10. Bound BOG, Dex and CHAPS molecules (from PDB codes 1M2Z, 7YXP, 4UDD and 7YXO, respectively) are shown as colored sticks, with cyan carbon atoms. (**F**) Subsite S2 features residues from the N-terminal half of H9, Phe715 / Thr719 in H10, and extends towards the C-terminal F domain (e.g., Phe774). BOG and JZR molecules (PDB codes 1M2Z and 3K22, respectively) are indicated as color-coded sticks with dark blue C atoms. (**G**) Subsite S3 binds the LSJ molecule (PDB 4LSJ) - represented as color-coded sticks with pale green C atoms - and includes the triplet of aromatic residues at the N-terminus of H10 together with His775. **H**, Relationships between BF-3 and S subsites at the top interface of GR-LBD. The boundaries of the subsites are shown in the left panel, colored as in figures 1D-G. The four surfaces are shaded in the central panel, with selected compounds shown as color-coded sticks. Note that subsite S1 matches the computationally identified cavity that is

12

202 only second to the LBP in terms of druggability (left panel). (See Fig. S1 for the surface topography

203 of other NRs and Table S1 for more details).

A surface-exposed cavity lined by helices H9 / H10 and the connecting loop is a common

binding site for small molecules

206 Given the high ligand affinity and significant druggability predicted for some solvent-

207 exposed cavities in GR-LBD, we explored the crystallographic evidence that supports their

208 capacity to bind small molecules. In our recently reported structures of GR-LBD, we unexpectedly

209 observed extra electron density at the 'top' homodimerization interface of the domain, which could

210 be interpreted as either the commonly used bile acid-derived detergent, CHAPS, or as a Dex

211 molecule (PDB entries 7YXO and 7YXP[13]) (Fig. 1, B and C). The observation of these cholesterol-

212 derived compounds bound to a BF-3–proximal surface prompted us to systematically review

213 deposited crystal structures for small molecules bound to the GR-LBD surface. The results of this

214 analysis are summarized in Fig. S1, B to D, and reveal three different subsites that overlap with

215 the 'top' interface of GR (labeled S1 to S3 in Fig. 1, E to H)[13]. Notably, the conformation of the

216 Trp712 indole moiety varies to accommodate these small molecules in the different crystal

217 structures (Fig. S1, B and C). Subsite S1, which corresponds to the most prominent cavity

218 identified in our bioinformatics analyses (Tables S1-S3), is a major binding site for molecules

219 featuring from one to three rings. This cavity exhibits notable flexibility and adaptability, as

220 evidenced by variations in the solvent-accessible surface area across the various crystal structures

221 (Fig. S2A). Moreover, the electrostatic potential of the GR-LBD surface reveals that this region is

222 predominantly neutral, providing an optimal environment for ligand docking through hydrophobic

223 interactions (Fig. S2B). Because binding to this solvent-exposed groove could regulate GR

224 biological activity in living cells (see below), we designated the subsite S1 as 'sensor function-3

225   (SF-3)', with S2 and S3 as lateral extensions of this cavity. SF-3 comprises residues from helices

226   H9/H10 and the connecting loop, most notably a triplet of conserved aromatic residues at the N-

227   terminus of H10 (Trp712, Phe715 and Tyr716; Fig. 1D). SF-3 is thus contiguous to but

228   topologically distinct from the BF-3 pocket[15,29]. Another noticeable surface cavity formed by

229   neighbouring residues of the L1-3 loop (e.g., Trp557), L6-7/H7 (e.g., Met639, Cys643), and helix

230   H11 (most notably Tyr735) was also identified as binding site for small molecules in several

231   crystal structures. This pocket has been postulated as a hormone entrance channel to the LBP in

232   several NRs[79], and therefore will be termed entry/exit (E) site in the following (Fig. S1D).

233   Several observations from previous crystal structures solved at higher resolution are

234   particularly noteworthy. (1) In addition to CHAPS, molecules of other non-ionic detergents, octyl

235   β-D-glucoside (BOG) and hexyl β-D-glucoside (HOG), occupy SF-3 in entries 1M2Z[10] and

236   3K22[80], respectively (Fig. S1B). (2) Some GR-LBD modules feature up to three bound CHAPS

237   molecules. One of these detergents, which overlaps well with the multiring ligands found in our

238   crystals, docks on helix H9 with its head trapped between the aromatic side chains of Trp712 and

239   Phe715 (4UDD[81]) (Fig. S1B). A second binding site for CHAPS is observed in this structure and

240   in entries 4UDC, 5G3J[82], and 5NFP[83], which overlaps with the E site (Fig. S1C and D). Finally,

241   and particularly relevant for its pharmacological implications, (3) two molecules of the

242   nonsteroidal GC, LSJ, occupy both the LBP and SF-3 in entry 4LSJ (Fig. S1B); the latter making

243   strong contacts with the Trp712 / Phe715 / Tyr716 triplet[84]. Interestingly, temperature factors for

244   both GC molecules are similar (average B factors 22.7 vs. 27.8 $Å^2$), highlighting the strong binding

245   of the compound to SF-3. Overall, while ligand binding relies mostly on Van der Waals (VdW)

246   contacts, several polar/charged residues in SF-3 can engage in electrostatic interactions (e.g.,

247   Ser708 and Asn711), providing specificity for ligand recognition.

248   The SF-3 site participates in important homo- and heterotypic interactions. Most notably,

249   SF-3 residues are involved in several of the 20 possible arrangements of GR-LBD homodimers in

250   our recently presented catalog[13]. This is in addition to several symmetric, parallel homodimers in

251   which the H10 aromatic triplets of two monomers contact each other[85], thus effectively juxtaposing

252   their SF-3 pockets. The gathering of the six exposed aromatic side chains (Trp712/712',

253   Phe715/715', and Tyr716/716') generates large cavities with potential higher ligand binding

254   capacity. In fact, head and tail of the best-defined BOG molecule in 1M2Z occupy the SF-3 pockets

255   of neighbouring monomers. These observations suggest that occupancy of SF-3 by small-molecule

256   compounds could modulate self-assembly of the full-length receptor. Furthermore, the recent cryo-

257   EM structure of the human GR-Hsp90-p23 complex reveals that p23 directly interacts with this

258   hydrophobic patch, stabilizing native GR and enhancing hormone binding (Fig. S1E)[28].

Analog screening identifies bile acids as preferred SF-3 ligands

259

260 To further explore the binding potential of the solvent-exposed SF-3 pocket, we performed an

261 analog search across the 8 million compounds deposited in the ZINC and DrugBank databases,

262 focusing on structural and chemical similarities to cholesterol-derived molecules. Using both

263 fingerprint and substructure-based approaches, we identified 36 Dex and CHAPS analogs as

264 potential GR-LBD ligands (Table S4). The high prevalence of bile acids among the identified

265 molecules suggests that the SF-3 cavity is a preferred binding site for these cholesterol derivatives.

266 In addition, analog searches guided by the bound BOG molecules identified several polyphenols

267 with known anti-inflammatory activity as potential SF-3 interacting molecules (Fig. S2C and Table

268 S4).

269 Analogs for which structures were available were docked into the SF-3 cavity of human

270 GR-LBD (PDB 4UDD) using different constraints. Lithocholic acid (LCA) and other bile acids

271 fitted perfectly into SF-3 without clashes with the protein (Fig. 2, A to C). Notably, three of the

272 top analogs selected for the presence of a hydrogen bond with the Ser708, as seen in the crystal

273 structure, formed additional salt bridges between carboxylate or sulfonate moieties of the bound

274 bile acid and the Arg690 guanidinium group, underscoring their strong electrostatic

275 complementarity to SF-3. These observations suggest that conjugated bile acids with longer, acidic

276 tails might bind more tightly and with higher specificity to this cavity. Docking experiments with

277 AlphaFold3 (Fig. S2D) and AutoDock (Fig. S2E) suggested that LCA could dock inside the LBP

278 of human GR-LBD, with only minor clashes with residues such as Met604 and Phe623. However,

279 most AutoDock runs locate the bile acid outside the LBP. Furthermore, closer inspection of these

280 docking poses reveals that LBP-bound LCA molecules would not be able to engage in H-bonds

281 with the Gln570 carboxamide group as in crystal structures of Dex/Cort-bound GR-LBD (Fig.

282 S2F). Binding of conjugated bile acids such as taurocholic acid (TauroCA) inside the LBP would

16

283 be even less favorable, as it would require substantial rearrangements of the LBP, and no such

284 docking solutions were found (Fig. S2, G to I). Of note, AlphaFold3 predictions of TauroCA

285 binding to human GR-LBD in the presence of Cort show the E and SF-3 cavities as preferred

286 binding sites for the bile acid. Predicted binding energies of these interactions calculated by

287 pyDock scoring suggest a more favorable ligand binding to SF-3 compared to the E site (-12.0 vs.
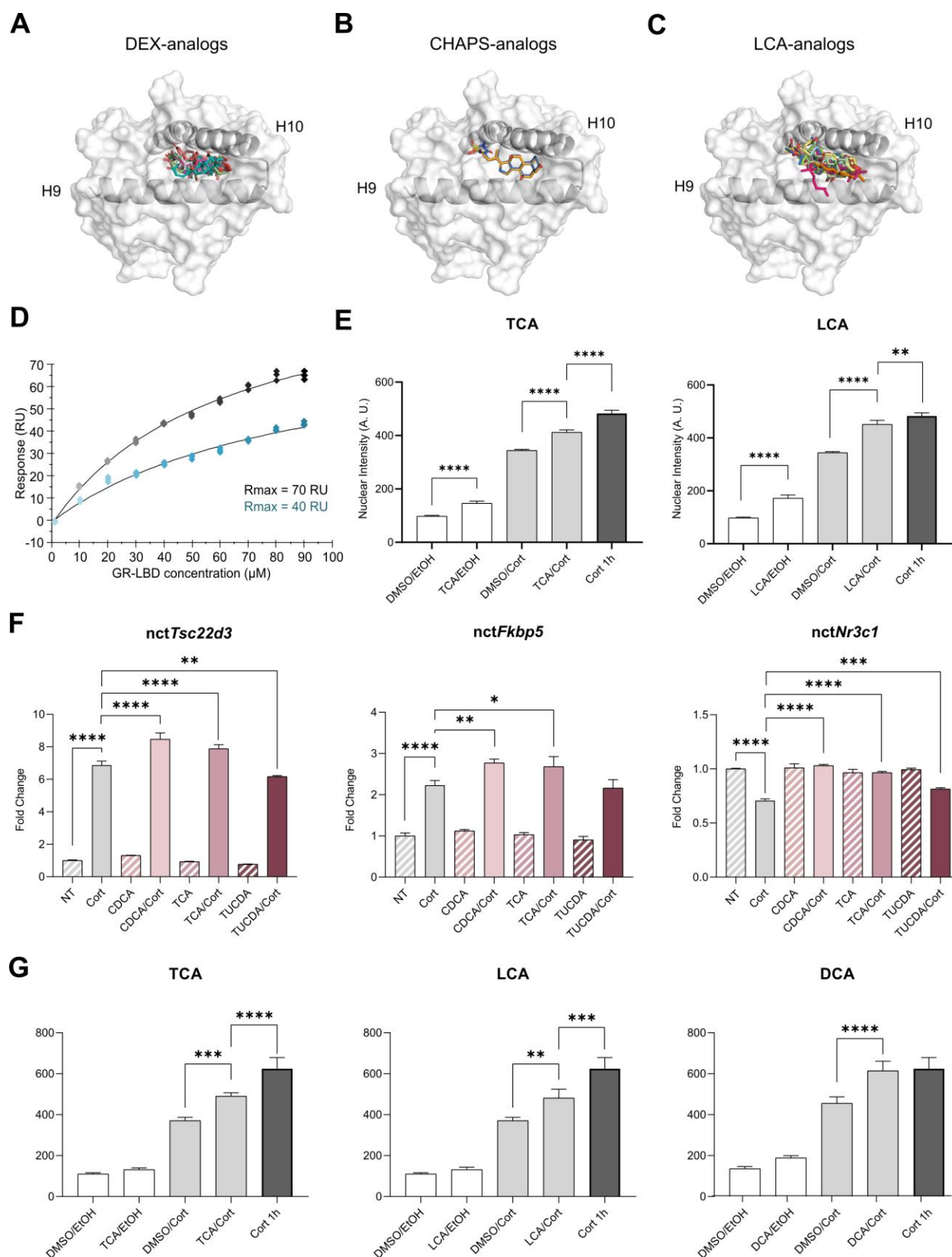
288 -9.9 kcal/mol, Fig. S2J).

17

A DEX-analogs

B CHAPS-analogs

C LCA-analogs

D

Rmax = 70 RU
Rmax = 40 RU

E TCA

LCA

F nct*Tsc22d3*

nct*Fkbp5*

nct*Nr3c1*

G TCA

LCA

DCA

289

18

290 **Fig. 2. Bile acid binding to GR-LBD reduces self-association in solution, reverts the Cort-**

291 **mediated negative feedback loop in cells and protects GR from proteasomal degradation.**

292 **Fig. 2 Legend**. **A-C**, Several multiring compounds, most notably bile acids, were identified as SF-

293 3 binders in high-throughput docking experiments conducted using either Dex (**A**), CHAPS (**B**) or

294 LCA (**C**) as templates. The top compounds identified in these screens are represented as colored

295 sticks. **D**, LCA binding to GR-LBD interferes with protein self-association in solution. SPR

296 experiments were performed by running increasing concentrations of Dex-bound GR-LBD (0.2,

297 0.4, 0.8, 1.6, 3.12, 6.25, 12.5 and 25 μM) in the presence or absence of LCA over chip-immobilized

298 GR-LBD. The fitted curves correspond to duplicate experiments conducted in the absence (black)

299 or presence (blue) of 40 μM LCA. Protein-protein self-association was analyzed according to a

300 1:1 model. The results of assays conducted in triplicate are shown along with the respective

301 maximum response. **E**, Nuclear intensity levels of endogenous GR after bile acid incubation for

302 24 h in 3134 cells assessed by immunofluorescence staining (Ab: G-5). Cotreatment with 100 nM

303 Cort and 100 μM TCA or LCA leads to a significant increase in nuclear GR protein compared to

304 vehicle. Statistical analysis was performed using one-way ANOVA followed by Tukey's post-hoc

305 test to compare group means. Significant differences at p values < 0.05 are denoted by asterisks (*

306 $p < 0.05$, ** $p < 0.01$, *** $p < 0.001$ and **** $p < 0.0001$). **F**, Impact of 24 h treatment with 100

307 μM of the indicated bile acids on GR transcription, assessed by RT-qPCR. Mean relative

308 expression levels are normalized to a housekeeping gene (*18-S*), with error bars indicating standard

309 deviations from three biological replicates. Statistical analysis was performed using one-way

310 ANOVA followed by Tukey's post-hoc test to compare group means. Significant differences at p

311 values < 0.05 are denoted by asterisks (* $p < 0.05$, ** $p < 0.01$, *** $p < 0.001$ and **** $p < 0.0001$).

312 **G**, Nuclear intensity levels of Halo-TMR ligand-stained endogenous Halo-GR in 3134 cells was

313 measured after cotreatment of Cort and bile acid for 24 h and compared to Cort/DMSO (24 h). As

314   an additional control, untreated Halo-TMR-stained cells were cultured for 24 h in serum-free

315   medium and activated with Cort for 1 h to account for the loss of ligand-stained Halo-GR due to

316   the culturing in a serum-free medium (Cort 1 h). Statistical analysis was performed as described

317   above (E).

Bile acids and non-ionic detergents bind to immobilized GR-LBD and interfere with receptor

self-association in solution

320   To explore the possible functional relevance of small-molecule binding to GR-LBD and its

321   implications for receptor multimerization, we performed surface-plasmon resonance (SPR) assays

322   to verify whether cholesterol-related compounds and other non-ionic detergents might directly

323   influence homotypic interactions in solution (see Fig. S3A for the chemical structures of CHAPS

324   and tested bile acids). First, we verified that detergents CHAPS and BOG bind to immobilized,

325   Dex-bound GR-LBD with micromolar affinity (Fig. S3, B and D). Next, we assessed whether these

326   compounds could modulate GR-LBD protein-protein interactions in solution. To this end, we

327   conducted further SPR experiments in which the binding sites in the immobilized GR-LBD were

328   first saturated with detergent (1 mM CHAPS or BOG). Then, increasing concentrations of GR-

329   LBD were run over the Biacore chip, also in the presence of buffers supplemented with the same

330   saturating detergent concentrations. Indeed, saturation of CHAPS binding sites led to a two- to

331   three-fold decrease in the strength of protein-protein interactions, depending on the model used to

332   fit SPR data, when compared to our previous results for WT GR-LBD[13] (Fig. S3C). By contrast,

333   no significant effects on the 1:1 interaction were detected in the presence of BOG (Fig. S3E).

334   These results demonstrate that cholesterol-derived detergents such as CHAPS can bind GR-LBD,

335   likely to SF-3, and interfere with GR-LBD self-association in solution. Importantly, two

336   physiologically relevant bile acids, LCA and TauroCA, bound to GR-LBD with higher affinity

337   than CHAPS (k_D = 4.9 and 6.0 µM, respectively; Fig. S3, F and G). Furthermore, incubation of

338   saturating concentrations of LCA interfered with GR-LBD self-association, reducing the

339   maximum response by over 40% (Fig. 2D).

340   **Long-term treatment with bile acids protects GR from hormone-induced repression and**

341   **proteasomal degradation**

342   Given the structural and computational evidence indicating that bile acids are preferred SF-3

343   ligands and have an impact on GR-LBD self-association in solution, we decided to explore their

344   potential impact on the turnover of the full-length receptor. The SF-3 pocket is recognized by the

345   Hsp90-p23 chaperone complex, which plays an essential role in maintaining the folded state of

346   GR, preventing its premature degradation[28]. E3 ligases like CHIP recognize and ubiquitinate free

347   GR, which is followed by its proteasomal degradation[86,87]. Serum bile acid concentrations in

348   humans can vary significantly based on factors such as age, gender, and health conditions. In

349   healthy individuals, total serum levels are typically below 5 µM. However, in certain pathological

350   conditions, bile acid levels can rise substantially, reaching concentrations over 100 µM[88–90].

351   Intracellular levels of bile acids are more challenging to measure and can vary significantly

352   between different cell types and pathophysiological conditions[91].

353   To assess whether bile acids can interfere with this process, we treated 3134 mouse

354   mammary adenocarcinoma cells with 100 nM Cort in the presence or absence of 100 µM non-

355   conjugated (deoxycholic acid; DCA, LCA, CDCA) or taurine-conjugated bile acids, (TauroCA,

356   TauroUDCA) for 24 h and measured the expression levels of endogenous GR by

357   immunofluorescence staining. GR protein levels were higher both in the nucleus and the cytoplasm

358   compared to untreated controls (Fig. 2E and S4A, B). We also detected an increase in the

359   expression levels of nascent *Fkbp5* and *TTscc22d3* genes after bile acid treatment for 24 h (Fig.

360   2F), indicating that the higher GR concentrations affect its transcriptional outcome. To discern

361 whether the effects of long-term treatment with bile acids are due to protection from protein

362 degradation or because of an increase in GR transcription, we performed qPCR analysis of nascent

363 *Nr3c1* under the same conditions. The results show a decrease in GR expression after 24 h of Cort

364 induction (Fig. 2F), which is in line with previous observations of an inhibitory feedback loop

365 triggered by prolonged hormone activation[92–94]. The observed Cort-repression was reverted when

366 co-treating with bile acids for 24 h, suggesting that these cholesterol-derivatives counteract GC-

367 triggered inhibitory feedback mechanisms.

368   To assess whether bile acids could independently affect GR protein stability, we performed

369 additional experiments with cells expressing Halo-tagged endogenous GR essentially as described

370 above. Labeling with the specific fluorescent HaloTag ligand, TMR, enabled us to selectively track

371 pre-existing receptor molecules, thus avoiding interference from newly synthesized protein.

372 Quantification revealed a significant increase in TMR signal in cells treated with LCA, DCA or

373 TauroCA compared to untreated controls (Fig. 2G), indicating that bile acid treatment protects GR

374 from degradation over the 24-hour period. Taken together, our results suggest that long-term

375 incubation with bile acids not only interferes with the hormone-induced negative feedback that

376 typically represses GR gene expression but also stabilizes GR protein by preventing its

377 proteasomal degradation, demonstrating dual modulation at both transcriptional and post-

378 translational levels.

379 **Short-term treatment with bile acids downregulates GR transcriptional activity**

380 Long-term treatment with both conjugated and non-conjugated bile acids potentially inhibits Cort-

381 induced repression of *Nr3c1* expression (Fig. 2E-F and Fig. S4). Therefore, we decided to further

382 explore their impact on the short-term transcriptional activity of GR. We first tested whether these

383 cholesterol-like compounds could affect early human GR transcriptional activity after GC

384 induction. For that, we treated human leukemic monocyte THP1 cells with 10 nM Dex, alone or

385   in combination with 20 µM CHAPS or LCA. As expected, Dex potently induced expression of

386   *Tsc22d3*, when compared to non-stimulated cells. However, this effect was suppressed in the

387   presence of the cholesterol derivatives (Fig. S4C). Subsequent experiments were carried out with

388   3134 mouse mammary adenocarcinoma cells, as they were also used for assessing GR dynamics

389   and function in living cells (see below).

390   We assessed the impact of three secondary bile acids on early GR function: LCA, the

391   closely related UDCA, and TauroCA, with a longer tail and a terminal sulfonate group due to its

392   conjugation with taurine (see Fig. S3A for the chemical structures of the tested compounds). Of

393   note, concentrations of 100-200 µM of LCA and UDCA have previously been shown to possess

394   anti-inflammatory activity in colonic epithelial cells and to confer protection from colonic

395   inflammation *in vivo*[95]. We treated GR knock-out cells derived from the 3134-mouse mammary

396   adenocarcinoma cell line (3134-GR[KO]) expressing GFP-tagged mouse GR with different

397   concentrations of these bile acids for 2 h. Then, we analyzed the expression levels of several

398   classical GR target genes (*Per1*, *Tsc22d3*, *Sgk1* and *Arld4*) by qPCR. To prevent excessive GR

399   activation, we treated these GFP-GR expressing cells with a low, more physiologically relevant

400   concentration of Cort (100 nM). Pre- and co-treatment with different concentrations of all three

401   bile acids led to a significantly reduced expression of *Per1* and *Sgk1* genes, indicating an

402   antagonistic effect on GR transcriptional activity under these conditions (Fig. 3A). This

403   modulatory effect was not observed when higher Cort concentrations (400-600 nM) were used, or

404   when cells were stimulated with 100 nM of the more potent, synthetic GC, Dex (Fig. S5).
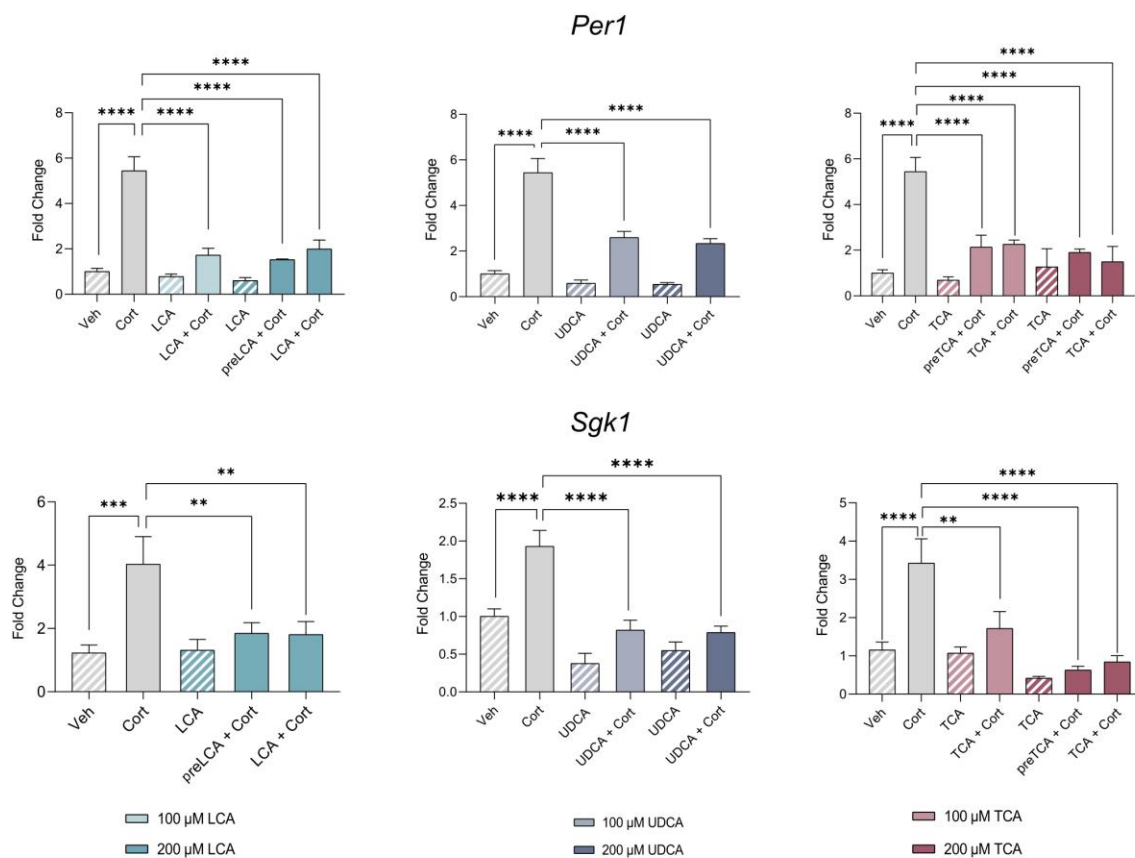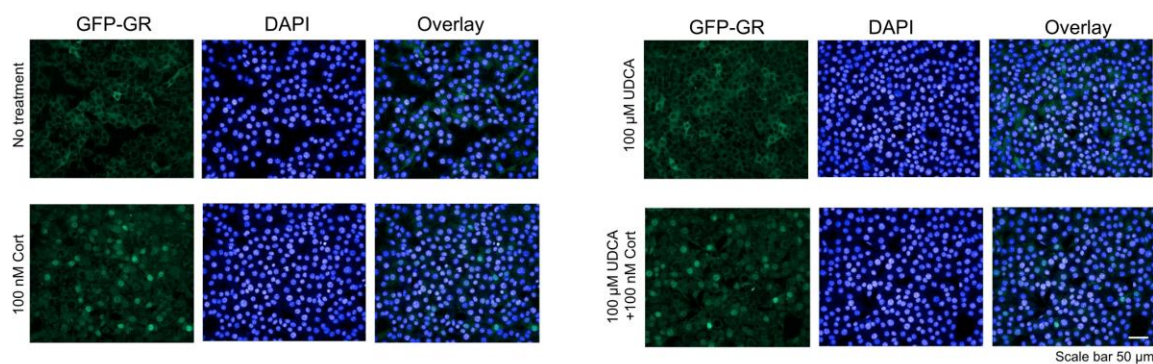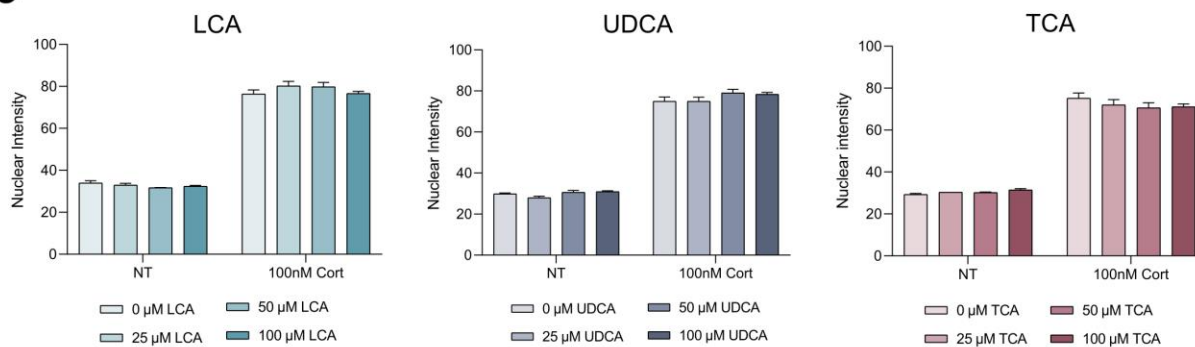
Fig. 3. Bile acids downregulate GR transcriptional activity without affecting its nuclear trafficking.

Fig. 3 Legend. A, Effect of 2 h treatment with bile acids on the expression of two major GR-responsive genes, *Per1* (top) and *Sgk1* (bottom), as assessed by RT-qPCR. Mean relative expression levels are normalized to a housekeeping gene (*β-actin* or *18-S*), with error bars indicating standard deviations from three biological replicates. Statistical analysis was performed using one-way ANOVA followed by Tukey's post-hoc test to compare group means. Significant differences at p values < 0.05 are denoted by asterisks (*p < 0.05, ** p < 0.01, *** p < 0.001 and **** p < 0.0001). **B**, Representative images of GFP-GR nuclear translocation in 3134 cells in response to 100 nM Cort, 100 μM UDCA, or both. Nuclei were stained with DAPI. Scale bar, 5 μm. **C**, Quantitative analysis of GFP-GR nuclear translocation upon incubation with either non-conjugated (LCA, UDCA) or conjugated bile acids (TauroCA, TCA). Translocation rate was calculated as the ratio of nuclear versus cytoplasmic intensity and each value was normalized to the control. Error bars represent the mean value ± standard error of the mean, n = 6.

Bile acids do not influence GR trafficking to the nucleus

The negative impact of bile acids on GR function in living cells could result from their interference with GR translocation to the nucleus. To explore this possibility, we assessed the translocation efficiency of cells treated with LCA, UDCA or TauroCA for 1 h, as compared to unstimulated cells (Fig. 3, B and C). Bile acid treatment alone did not promote GR translocation to the nucleus, indicating that, unlike steroid hormones, these cholesterol derivatives do not occupy the ligand-binding pocket of the receptor in a productive conformation. These results further validate the docking experiments and current crystallographic evidence described above and are in line with bile acids binding to SF-3 in living cells. Furthermore, GR translocation induced by Cort was not

429   affected by co-treatment with any of the tested bile acids (Fig. 3C). Thus, short-time treatment

430   with bile acids interferes with GR activity specifically in the nucleus.
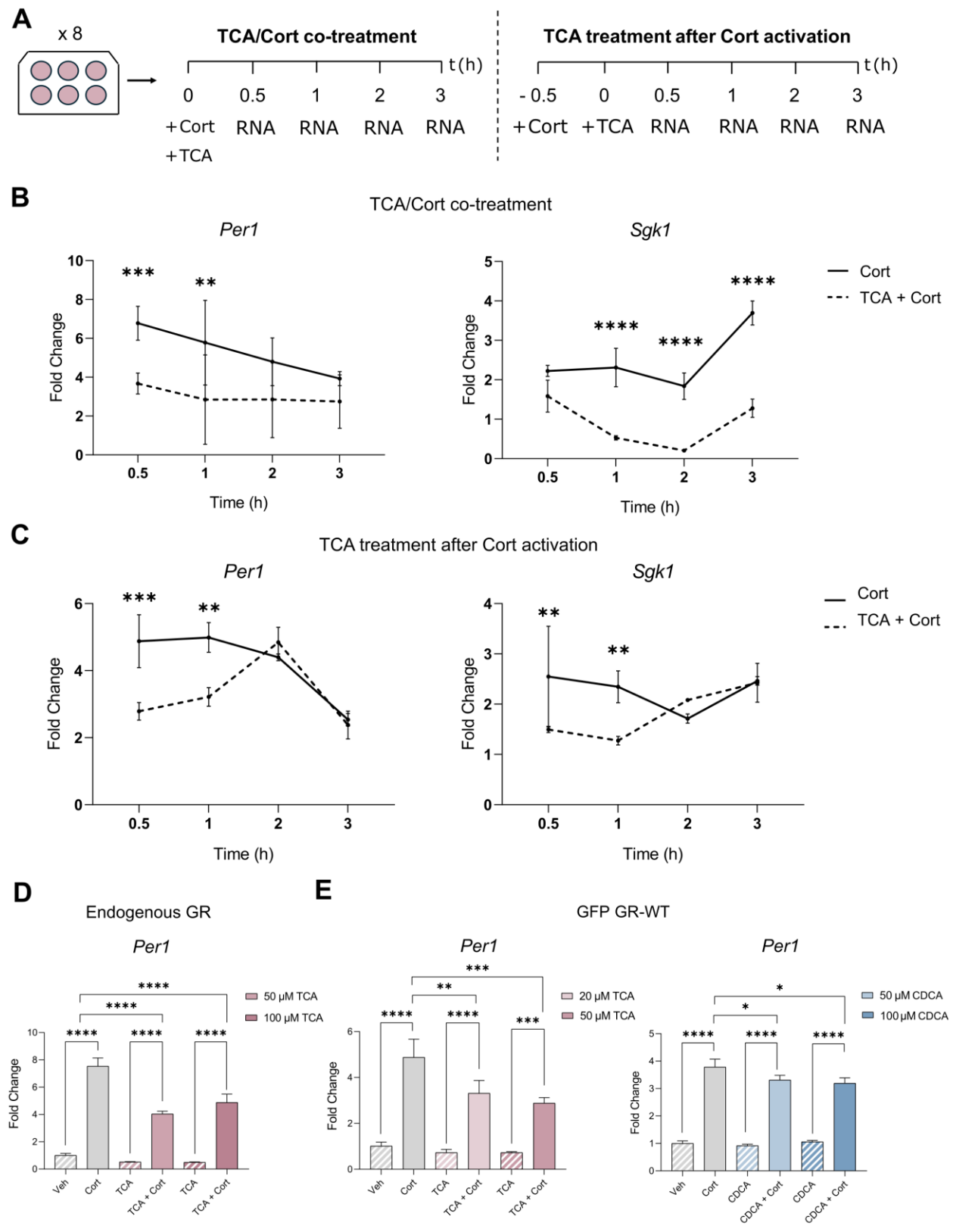
431

432

Fig. 4. Bile acids specifically downregulate the nuclear activity of GR.

Fig. 4 Legend. **A, B**, Time course of *Per1* and *SGK* gene expression (from 0.5 to 3 hours) as assessed by RT-qPCR. Cells were either cotreated with 100 nM Cort and 100 µM TauroCA (TCA) (**B**) or treated first with the hormone for 30 min before bile acid addition (**C**). Note the faster induction of *Per1*, which shows a maximum response 30 min after induction in both scenarios. Note also that the bile acid effect is significant at the time points of maximum gene expression. **D**, Downregulation of *Per1* gene expression after 30-minute co-treatment of 3134 cells, expressing endogenous GR, with 100 nM Cort and either 50 or 100 µM TauroCA. **E**, *Per1* expression is downregulated in cells expressing GFP-tagged GR by co-incubation with 20 or 50 µM TauroCA and 50 or 100 µM CDCA. Mean relative expression levels for all the experiments shown in panels A-D were normalized to a housekeeping gene (*β-actin* or *18-S*), with error bars indicating standard deviations from three biological replicates. Statistical analysis was performed using one-way ANOVA followed by Tukey's post-hoc test to compare group means. Significant differences ($p < 0.05$) are denoted by asterisks (*$p < 0.05$, ** $p < 0.01$, *** $p < 0.001$ and **** $p < 0.0001$).

Bile acids interfere with GR function at the chromatin level

To verify that bile acids affect GR once the receptor is translocated into the nucleus, we first compared the expression levels of *Per1* and *Sgk1* at various time points ranging from 0.5 to 3 hours after a 30 min activation with Cort alone or in combination with 100 µM TauroCA (see Figure 4A for a schematic representation of the experimental protocol). A significant reduction in expression levels was observed at the peak of induction for both genes in cells co-treated with TauroCA (*Per1* after 0.5 and *Sgk1* after 3 h), indicating that the bile acid rapidly downregulate GR activity and sustain this inhibitory effect over several hours (Fig. 4B). Then, we conducted the same experiment but adding TauroCA 30 min after Cort activation, thus ensuring a complete translocation of GR

456   into the nucleus before bile acid treatment. The results of this time-course assay showed a similar

457   reduction of *Per1* and *Sgk1* expression levels compared to previous conditions (Fig. 4C),

458   corroborating that the bile acid primarily affects GR function after its localization to the nucleus.

459   Additional experiments using 3134 cells expressing endogenous GR demonstrated that the

460   downregulatory activity of the bile acids was not conditioned by the GFP tag (Fig. 4D).

461   Additionally, we assessed whether the observed effects were maintained at lower bile acid

462   concentrations. Indeed, concentrations as low as 50 µM of the non-conjugated bile acid, CDCA,

463   or 20 µM of TauroCA were able to significantly reduce *Per1* expression (Fig. 4E), demonstrating

464   potent bile acid-mediated downregulation of GR transcriptional activity.

465   To further analyze the impact of bile acids on GR upon nuclear translocation, we conducted

466   single-molecule tracking (SMT) experiments[96] to follow the intranuclear dynamics of GR within

467   living cells in the presence or absence of TauroCA. SMT has emerged as a cutting-edge technology

468   for directly visualizing and tracking individual proteins in living cells, particularly transcription

469   factors[97]. Recent studies emphasize the importance of considering both specific and non-specific

470   protein-chromatin interactions when interpreting transcription factor movement and further

471   transcriptional activity[97]. We performed SMT on 3134 cells expressing HaloTag-mGR or Halo-

472   H2B chimeras (with H2B serving as a probe for photobleaching) to determine the spatial mobility

473   of these proteins in the nucleus after 1 or 3 h treatment with 100 µM TauroCA. Since LCA can

474   modulate GR oligomerization in solution (Fig. 2D), we performed SMT experiments in cells

475   expressing HaloTag-mGR P481R (also known as GR[tetra], a constitutively tetrameric GR

476   mutant)[98,99]. As shown previously, GR-WT and GRtetra exhibit power-law distributed dwell

477   times[100]. TauroCA significantly reduces the dwell time of WT GR after 1 hour of treatment (Fig.

478   5C), pointing to either a reduction in receptor stability when binding to chromatin or an increased

479   dissociation rate. We observed that, in the absence of bile acid, the dwell times of WT GR and

480   GR$^{\text{tetra}}$ are comparable. However, no effect was observed for the tetrameric mutant after 1 hour of

481   TauroCA treatment (Fig. 5, C to E). These results suggest that bile acids cannot modulate GR

482   structure and function when receptor multimerization is enhanced (e.g., by modifying the inter-

483   monomer interfaces). We also examined the spatial mobility of GR in the presence and absence of

484   TauroCA and found GR to exhibit two distinct low-mobility states as described previously for GR

485   and other chromatin associated proteins[101–104]. However, the higher mobility state was slightly

486   reduced, without affecting the total bound fraction or the fraction of the lowest mobility state,

487   which is preferentially occupied by activated GR (Fig. S6, A and B).

488   A similar decrease in the dwell time of WT GR was observed when comparing 1 versus 3

489   hours of Cort treatment alone. In addition, TauroCA treatment does not affect GR dwell time after

490   3 hours, likely because of a significant reduction in the number of Cort-activated GR molecules

491   under these conditions. We have previously shown that GR mediates transcriptional regulation

492   through rapid receptor exchange and hormone recycling[105]. Thus, it is possible that prolonged

493   hormone treatment promotes receptor turnover, thereby reducing dwell time independently of the

494   bile acid. Overall, these findings show that bile acids rapidly interfere with GR chromatin binding

495   and suggest that these molecules can modulate GR dynamics at the chromatin level.

496
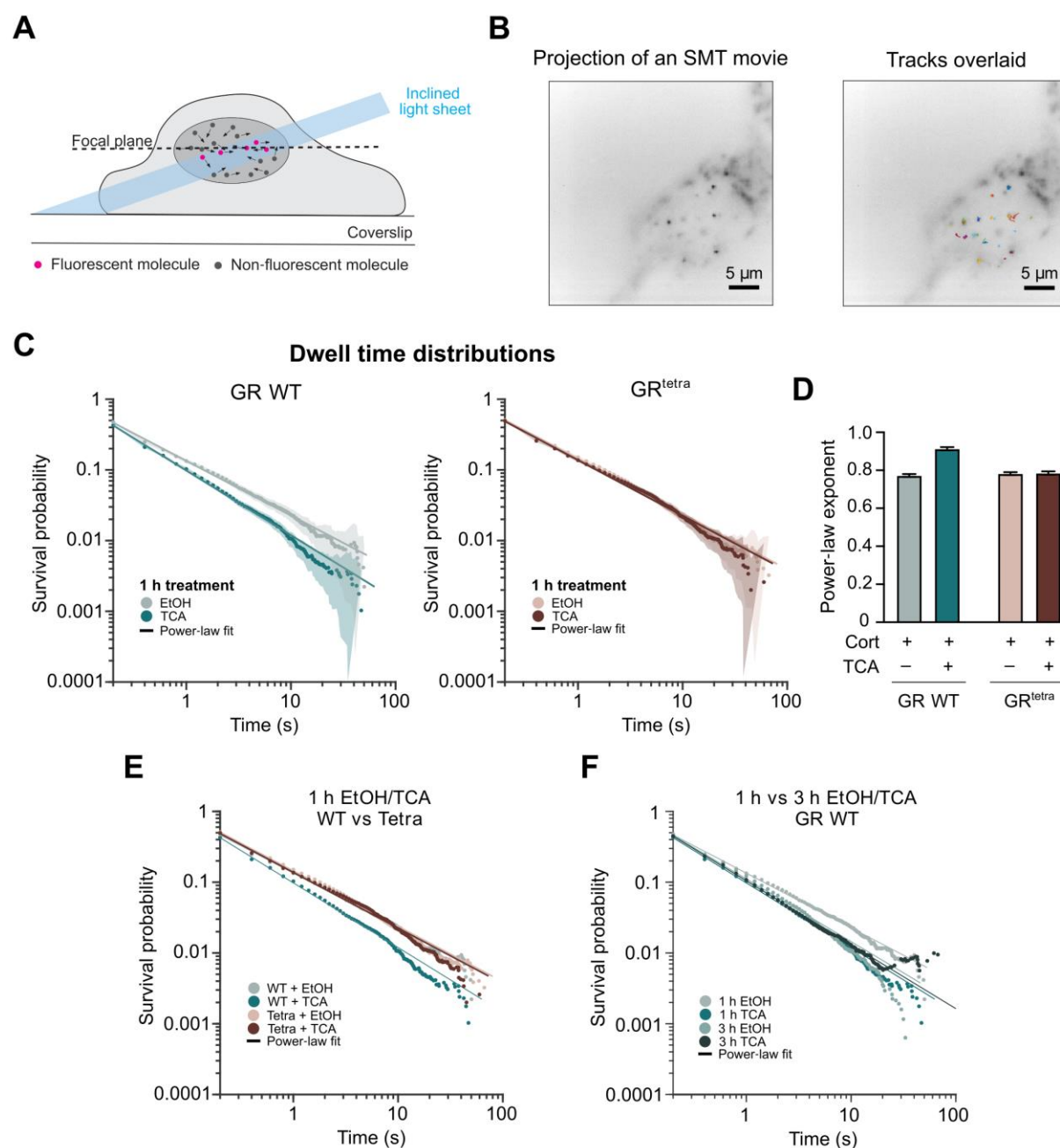
Fig. 5. Survival distributions of GR dwell times upon bile acid treatment.

Fig. 5 Legend. A, Schematic representation of the SMT setup using highly inclined and laminated optical (HILO) microscopy. A thin section of the sample is illuminated, reducing background fluorescence and enhancing signal-to-noise for single-molecule detection. Fluorescent molecules within the focal plane (magenta dots) are selectively excited and tracked. **B**, Time projection of a representative Halo-GR WT SMT movie (left panel) and tracks generated by the observed GR

503   molecules over time (right panel). **C**, SMT of Halo-WT GR and Halo-GR^{tetra} activated with 100

504   nM Cort (Ncells WT = 36, Ntracks WT = 9078, Ncells Tetra = 38, Ntracks Tetra = 18363), in the

505   presence or absence of 100 µM TauroCA (Ncells WT = 42, Ntracks WT = 13916, Ncells Tetra =

506   36, Ntracks Tetra = 15482). Images were collected every 200 ms with an exposure time of 10 ms.

507   The survival distributions are shown as solid lines, fitted to a power-law function. **D**, Power-law

508   exponent of Halo-WT GR and Halo-GR^{tetra} under different treatments with Cort and/or TauroCA.

509   Note that TauroCA cotreatment increases WT GR exponent compared to Cort alone, while no

510   differences are observed for GR^{tetra}. Error bars represent standard error of the mean (SEM). **E-F,**

511   Comparison of dwell time distributions between Halo-GR WT and Halo-GR^{tetra} after 1 (**E**) or 3

512   hours (**F**) of Cort activation, in the presence or absence of TauroCA.

513 **Taurocholic acid inhibits GR oligomerization and reduces its transcriptional activity in**

514 **living cells**

515 Current experimental evidence favors a pathway of GR activation that involves non-canonical

516 receptor dimerization upon GC binding and nuclear import, followed by its tetramerization when

517 bound to DNA[13,85,98,99] (summarized in Fig. 6A). Our recently presented structure of GR-LBD

518 from crystals with a very high solvent content revealed highly plastic tetrameric arrangements

519 (PDB entry 9HDF)[85]. These tetramers are formed by the association of pairs of non-canonical GR

520 dimers centered on loops L1-3 (core dimers) through their H9/L9-10/H10 surface, particularly SF-

521 3 residues Trp712 and Tyr716 (Fig. 6A)[85]. The significant plasticity at this dimer-of-dimers

522 interface allows different relative inter-dimer orientations, from more extended, 'open' to 'closed'

523 arrangements. These conformations have notably different SF-3 accessible areas, and therefore

524 different binding sites for small molecules (Fig. 6B). Demonstration that SF-3 preferentially

525 recruits cholesterol-derived molecules such as bile acids and biophysical evidence presented above

526 prompted us to explore their capacity to interfere with GR oligomerization in living cells. To this

527 end, we performed quantitative fluorescence microscopy (number and brightness, N&B) assays,

528 as previously described[99,106]. Briefly, 3134-GR[KO] cells were transiently transfected with GFP-

529 tagged GR and treated with 100 nM Cort, alone or in combination with 100 µM TauroCA. These

530 cells express a tandem array of DNA binding sites for GR, the mouse mammary tumor virus

531 (MMTV) array, to allow quantitative assessment of GR oligomeric state both in the nucleoplasm

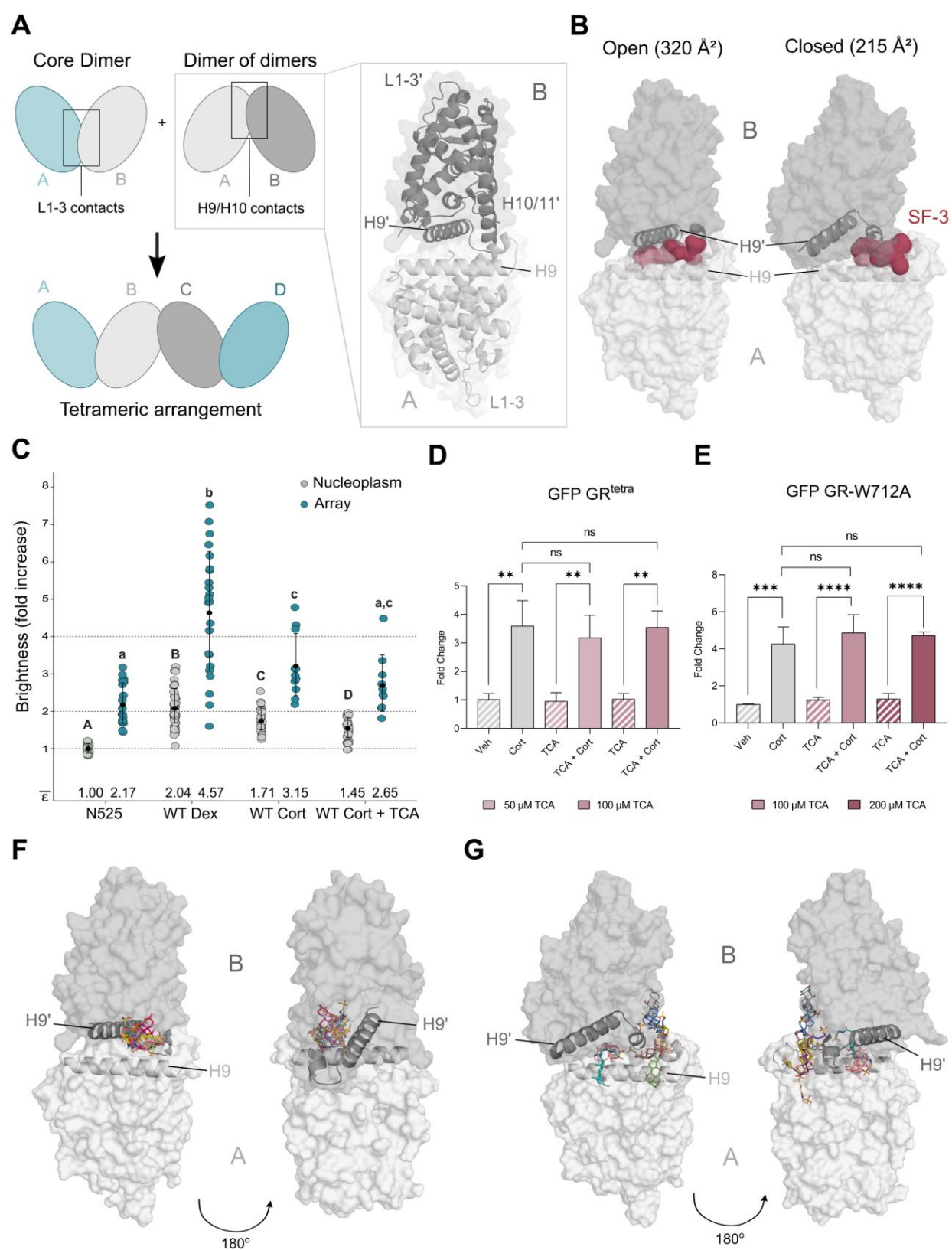532 and when bound to DNA (Fig. S6C).

533

Fig. 6. TauroCA modulates GR transcriptional activity in living cells by interfering with its self-assembly.

Fig. 6 Legend. A, Schematic representation of GR-LBD multimerization pathway. The core, non-canonical dimer is stabilized through L1-3 contacts, while interaction of two core dimers through the H9/H10 surface results generates a tetrameric arrangement (dimer-of-dimers). The zoomed-in structural view highlights key interface regions, including L1-3, H9 and H10/11. **B**, Open and closed conformations of GR-LBD dimer-of-dimers, indicating the variation in SF-3surface. **C**, FL GR oligomerization in the nucleus as assessed by N&B. The fold increase in molecular brightness (ε) relative to the N525* monomeric control is shown ($N = 134$ total cells with $10 < N < 33$ between experiments). Statistical analysis was conducted independently for molecules in the nucleoplasm and at the array (capital and small letters, respectively). Different letters indicate significant differences ($p < 0.05$, ANOVA and Tukey test; data from four independent microscopy sessions). **D-E**, *Per1* gene induction in a stable 3134-GR^{KO} cell line expressing (**D**) GFP-mGR^{tetra} or (**E**) GFP-mGR-W718A (W712A in hGR) after 30 min of 100 nM Cort treatment, alone or in combination with TauroCA, as assessed by RT-qPCR. Mean relative expression levels for all the experiments are normalized to a housekeeping gene (*β-actin*), with error bars indicating standard deviations from three biological replicates. Statistical analysis was performed using one-way ANOVA followed by Tukey's post-hoc test to compare group means. Significant differences ($p < 0.05$) are denoted by asterisks (*$p < 0.05$, ** $p < 0.01$, *** $p < 0.001$ and **** $p < 0.0001$). **G-H**, Results of ten independent docking runs of TauroCA onto the two conformations of the GR-LBD dimer-of-dimers. In the 'open' conformation (**G**), all runs consistently place the TauroCA molecule (colored spheres) within the extended SF-3. By contrast, in the 'closed' conformation (**H**) only one TauroCA molecule occupies this cavity, while the other four runs position the bile acid randomly along the dimerization interface.

558   Corticosterone treatment induced GR dimerization in the nucleoplasm and tetramerization

559   at the array as expected, although to a lower extent compared to Dex-stimulated cells (Fig. 5B).

560   When cotreated with TauroCA, Cort-induced dimerization and tetramerization of the nuclear

561   receptor were substantially impaired with an ε decrease from 1.71 to 1.45 and 3.15 to 2.65,

562   respectively (Fig. 6C). These results suggest that bile acids can disrupt the inter-monomer

563   interactions needed to form and stabilize GR tetramers by binding to SF-3.

564   To further explore the interplay between bile acid binding and receptor multimerization,

565   we took advantage of the constitutively tetrameric GR variant, GR^{tetra} [98,99]. We reasoned that the

566   multimerization behavior of this variant would be less affected by bile acid treatment compared to

567   WT, likely because SF-3 would be at least partially occluded within GR tetramers. To verify this

568   hypothesis, we first analyzed *Per1* expression in 3134-GR^{KO} cells expressing GFP-tagged GR^{tetra}

569   and treated with 100 nM Cort alone or in combination with 100 µM TauroCA. As expected, no

570   downregulation of GR function was observed for the constitutive tetrameric variant (Fig. 6D).

571   These results are in line with the lack of effect on chromatin binding observed for GR^{tetra} after

572   TauroCA treatment (Fig. 5C). To further explore this, WT-GR and GR^{tetra} were treated with 100

573   nM Cort and their transcriptional programs in the presence and absence of 100 µM TauroCA were

574   compared. Transcriptional activity of Cort-induced GR was reduced by more than 80% after

575   TauroCA treatment, whereas GR^{tetra} response was not affected (Fig. S6, D to F).

576   To verify that bile acids modulate GR tetramerization by binding to SF-3, thus interfering

577   with inter-monomer interactions between aromatic residues at the N-terminal end of H10, we

578   performed further experiments with the GR^{W712A} mutant (Trp718 in mouse GR). We have

579   previously shown that this truncation does not impair GR oligomerization on its own[13], but it

580   would alter the SF-3 architecture and reduce bile acid binding, allowing us to target this cavity

581   without altering central GR functions. In striking contrast to the results obtained with WT GR (Fig.

582   4B), *Per1* expression levels in cells expressing the GR^{W712A} mutant after 30 minutes of treatment

583   with 100 nM Cort were not affected by the presence of 100 µM TauroCA (Fig. 6E). These findings

584   strongly support our hypothesis that bile acids interact with GR in living cells mostly through SF-

585   3, thus interfering with GR tetramerization and chromatin binding and therefore with its

586   transcriptional activity.

587   To further explore bile acid binding modes to SF-3, we performed docking experiments of

588   TauroCA on monomeric GR-LBD and two distinct conformations of the "dimer of dimers"

589   generated by juxtaposition of the Trp712-centered interfaces from two monomers[85] (Fig. S5G and

590   Fig. 6, F and G). In the five independent docking runs on the open dimer, TauroCA was

591   consistently positioned within the SF-3 cavity (Fig. 6F), highlighting the accessibility of this

592   pocket to bile acids in this arrangement. In contrast, only one docking run on the closed

593   conformation positioned TauroCA within the SF-3 cavity, while the other nine placed the molecule

594   randomly along the dimer interface (Fig. 6G). Moreover, important clashes of the docked TauroCA

595   molecules with residues Lys695, Trp712, and Tyr716 can be observed when superimposing

596   molecules docked in the open arrangement on the closed conformation (Fig. S5H). Thus, the

597   reduced size and accessibility of the SF-3 pocket in the closed dimer-of-dimers of GR-LBD would

598   prevent effective bile acid binding.

DISCUSSION

Our findings illuminate previously unappreciated mechanisms through which bile acids modulate glucocorticoid receptor activity. While it has been assumed that bile acids can compete with GCs for the internal ligand-binding pocket of this nuclear receptor, our current structural and docking evidence indicates that this regulatory role is actually driven by the occupancy of well-defined cavities on the surface of the ligand-binding domain. Solvent-exposed surfaces enriched in hydrophobic/aromatic residues are primary binding sites for chaperones and cochaperones, but in isolated proteins, they recruit small molecules with detergent-like properties instead[18]. In line with this observation, a thorough bioinformatics analysis of the LBD surface and previous structural evidence reveals two major GR-LBD cavities as important bile acid targets, for which we have coined the terms SF-3 and E sites. The E site is spanned by residues of loops L1-3 / L6-7 and H11, while the SF-3 cavity is delimited by residues in helices H9/10 and the connecting loop, most notably the conserved aromatic residues at the N-terminus of H10, Trp712 and Phe715 (Fig. 1, D to H). Noteworthy, these cavities partially overlap with two major inter-monomer interfaces at the top and back of the GR-LBD module in the standard orientation (Fig S1B, C)[13,85].

Our current results indicate that both short- and long-term effects of bile acids on GR transcriptional activity are largely a consequence of the competition between bile acid binding and receptor self-assembly and underscore the importance of SF-3 in this regard. (1) N&B results show a direct impact of TauroCA binding on receptor di- and tetramerization (Fig. 6C), similar to what we have previously observed for SF-3 mutants, GR^{W712E} and $GR^{W712S/Y716S}$ [85]; (2) Chromatin binding and transcriptional activity of the WT receptor, but not of the constitutively tetrameric variant (GR^{tetra}), are altered by short-term bile acids treatment (Figs. 5C and S5F); (3) Bile acids are unable to downregulate GR transcriptional activity in cells stimulated with 100 nM Dex or 600 nM Cort (Fig. S2, D and E) suggesting that sustained GR activation promotes the formation of

623   stable tetramers leading to occluded bile acid binding sites; (4) Long-term bile acid treatment

624   protects GR from proteasomal-driven degradation and reverts corticosterone-induced repression

625   of *GR* expression.

626   The most common arrangements of GR-LBD dimers-of-dimers in our recently reported

627   structure of multimeric GR-LBD positions the SF-3 pockets of two monomers in close proximity,

628   thus generating a large, solvent-protected area enriched in aromatic residues[85]. This arrangement

629   has been observed in several additional crystal structures, some of which feature a detergent

630   molecule occupying the SF-3 cavity of two neighboring monomers[13]. These properties are

631   characteristic of so-called multichain binding sites, i.e., binding sites for small-molecule ligands

632   formed at the interface between two or more monomers[107,108]. These studies demonstrated that

633   residues within multichain binding-sites are better conserved overall than those involved in

634   forming single-chain binding sites. Indeed, the residues that span SF-3 are highly conserved in GR

635   across species, ranging from fishes to humans, most notably the triplet of aromatic residues in H10

636   (Fig. 1D). Our docking experiments revealed that bile acid molecules would bind across two

637   neighboring SF-3 sites in the more open arrangement of Trp712-centered dimers-of-dimers, as

638   observed in crystal structures (Fig. 1E). However, in the 'closed' conformation the bile acid moiety

639   would clash with residues of the second LBD monomer (Fig. S5H). Thus, bile acid binding would

640   interfere with the ratcheting of GR dimers-of-dimers hindering their ability to transition between

641   different relative conformations. This interference might impair optimal binding to chromatin

642   and/or dynamics of the transcription machinery, ultimately leading to the observed decrease in

643   transcriptional output. Altogether, our results suggest that bile acid binding to the GR tetramer is

644   highly dependent on the specific conformation of the Trp712 interface, with the accessibility of

645   the SF-3 cavity playing a crucial role in GR modulation.

646   GR relies on a complex interplay between chaperones (Hsp70/Hsp90), cochaperones (p23)

647   and immunophilins (FKBP51, FKBP52) to adopt its mature, transcriptionally active

648   conformation[28,109,110]. Notably, SF-3 overlaps with the binding site for cochaperone p23 (Fig.

649   S1E)[28]. We have observed that GR translocation to the cell nucleus is not impaired by bile acids,

650   but interference with GR-nuclear chaperone interactions might affect the proper cycling of the

651   receptor on chromatin[111], further contributing to the reduction in transcriptional activity by

652   potentially impairing its dynamic engagement with target gene loci. GR appears to depend on the

653   nuclear chaperone function as part of the nuclear quality control system (involving an interplay

654   with the ubiquitin-proteasome system) for its proper function as a transcription factor *in vivo* [105].

655   Of note, our current results after long-term treatment indicate that bile acids not only interfere with

656   the proteasomal-driven GR degradation but also inhibit a hormone-induced inhibitory feedback

657   loop[92–94]. A schematic summary of the manifold effects of bile acids on GR function *in vivo* is

658   shown in Figure 7.

659   The dynamic equilibrium between GR monomers and oligomers depends on the potency

660   of the LBP-bound glucocorticoid. Our N&B analysis, which allows for the *in situ* quantification

661   of GR oligomerization states in living cells indicates that the less potent natural GC, corticosterone,

662   has a lower ability to shift the equilibrium towards multimers compared to Dex. This balance is

663   significantly displaced towards oligomers for GR^{tetra}, and consequently, less dynamic. Thus, bile

664   acids have higher probability of interacting with WT-GR compared to GR^{tetra}, as the SF-3 cavity

665   is fully accessible in GR homodimers. The impact of bile acids binding to SF-3 on both

666   dimerization and tetramerization is also in line with allosteric rearrangements that extend to the

667   opposite pole of the domain, including the dimerization site centered on loop L1-3, as previously

668   observed by us and others[112,113]. Bioinformatic analyses revealed that the SF-3 cavity is unique for

669   GR, and even in the closely related MR, no evidence for small-molecule binding to the

670   topologically equivalent area has been reported to the best of our knowledge. Inspection of

671   deposited crystal structures of MR-LBD reveals a tight packing of monomers that leaves no space

672   for cholesterol-derived molecules close to the conserved Trp712/Phe715/Tyr716 triad (human GR

673   numbering; see e.g. the structures of MR-LBD bound to Cort, aldosterone or progesterone, PDB

674   entries 2AAX, 2AA2 and 2AA5, respectively[114]). These observations suggest that bile acids could

675   selectively modulate GR activity without affecting MR, highlighting a potential for targeted

676   regulation without cross-reactivity.

677   On the other hand, binding to the other major cavity on the GR-LBD surface, the E site is

678   likely to have direct effects by interfering with hormone trafficking in and out of the LBP, in

679   addition to impacting receptor multimerization. Direct physical interactions between small

680   molecules bound at the E site and inside the LBP have been reported. For instance, a HOG

681   molecule in PDB 3K22 makes VdW contacts with the bound GC (Fig. S1D)[80]. Direct contacts

682   between lithocholic acid that occupies the E site and the LBP-bound 4-hydroxy-tamoxifen have

683   also been reported for estrogen receptor-related γ (ERRγ) (PDB 1S9Q[115]; 7R62[116]).
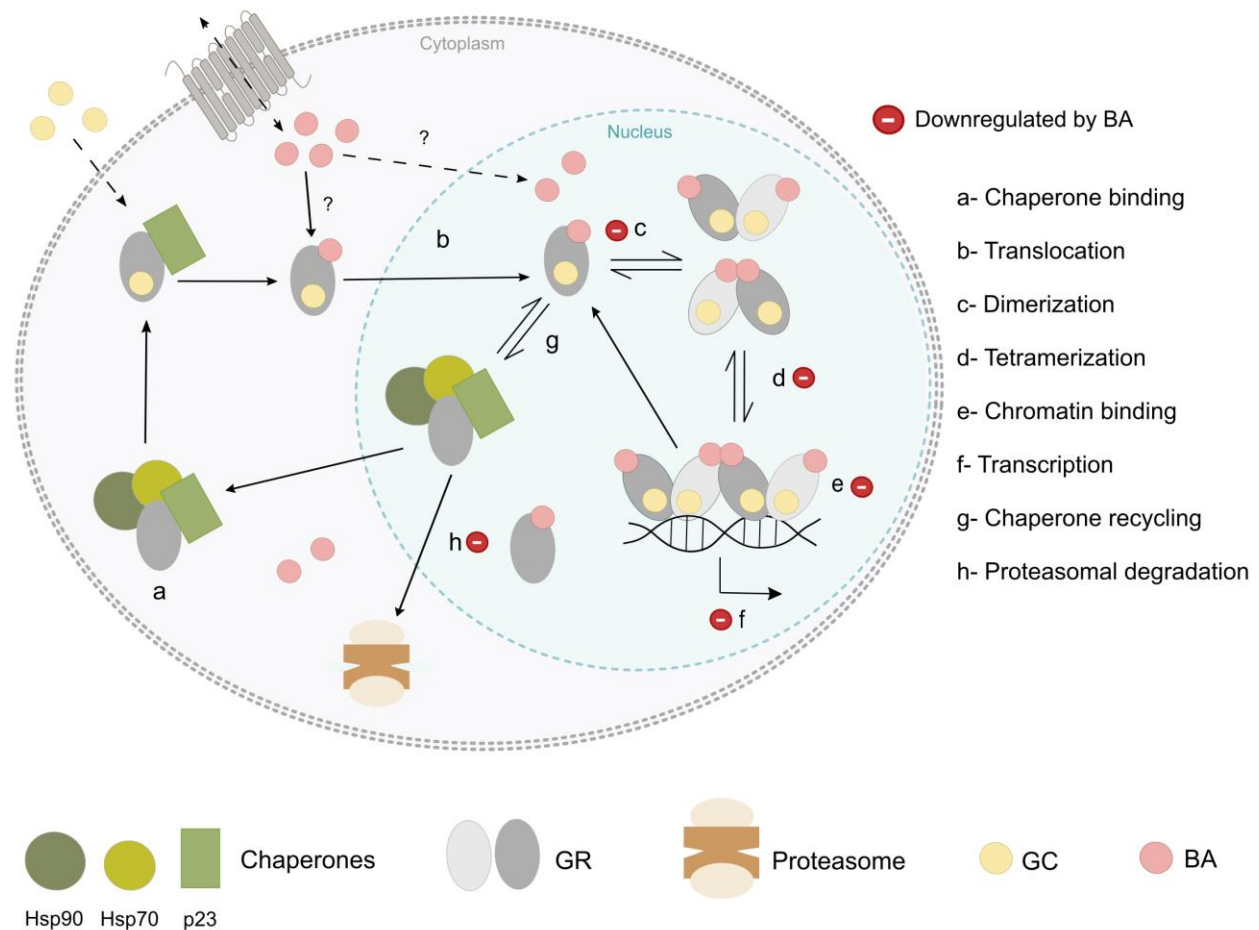
Fig. 7. Mechanisms of bile acid-mediated regulation of GR function.

Fig. 7 Legend. Schematic representation of bile acids effects on the life cycle of the glucocorticoid receptor. Bile acids can then either diffuse into the nucleus or be actively transported bound to other proteins, including GR[117]. In the cytoplasm, inactive GR is stabilized by a chaperone complex comprising Hsp90, Hsp70, and p23 (a). Upon glucocorticoid binding (GC, yellow circles), GR undergoes conformational changes and translocates into the nucleus (b). Inside the nucleus, GR forms dimers (c) which then associate into tetramers (d) upon chromatin binding (e). This leads to transcriptional activation of target genes (f). In the nucleus, GR cycles between GC-bound (active) and GC-free conformations, in a process that is also facilitated by the chaperone machinery (g). Finally, GR can be either exported to the cytoplasm or degraded by the proteasome (h). Current experimental data shows that bile acids (BA, pink circles) significantly downregulate

696 GR function in the short- and long-term by interfering with several of these key steps, including

697 receptor turnover, oligomerization, and chromatin binding (highlighted with a negative icon). By

698 interfering with GR structure and function at multiple levels, bile acids significantly impair GR-

699 mediated gene regulation, reducing its transcriptional activation of target genes. This is in addition

700 to the inhibition of Cort-initiated negative feedback loop.

701 We stress that bile acid concentrations used in our experiments in living cells are within

702 the range of those observed *in vivo*, mainly in pathological conditions such as cholestasis or liver

703 dysfunction[35,45,46,50,51,62,118,119]. In our hands, TauroCA showed a slightly higher impact on GR

704 transcriptional activity than bile acids such as LCA and UDCA. These functional differences are

705 most likely related to the presence of a longer, acidic taurine tail, which is capable of extending

706 towards the Arg690 side chain, engaging in salt bridge formation with its guanidinium group.

707 Future investigations should determine whether other secondary bile acids bind with even higher

708 affinity to GR-LBD, potentially exerting a greater impact on the transcriptional activity of the

709 receptor. Given the vast diversity of bile acids[119–121], it is tempting to speculate that direct and

710 specific links connect the gut microbiota with major physiological processes through direct

711 physical interactions with nuclear receptors[122].

712 This bile acid-mediated modulation of steroid receptors through binding to a solvent-

713 exposed cavity distant to the internal hormone-binding pocket is conceptually similar to exosites

714 identified in regulatory serine proteases[123]. This is in strong contrast to other previously

715 characterized BARs, FXR and VDR, and presumably other members of the NR1H and NR1I

716 subfamilies, in which bile acids occupy the internal LBP[58]. Interestingly, similar to the regulatory

717 serine proteases, dual binding modes have been previously reported for bile acids. Specifically,

718 binding of a second LCA molecule to the VDR surface was shown to be critical for LCA

719 agonism[17]. Current evidence indicates that bile acids play a central role by modulating the

43

720   intertwined relationship between the two groups of nuclear receptors, especially between GR and

721   FXR[124]. In this regard, LCA has been recently shown to mediate the effect of calorie restriction by

722   activating the master regulator of metabolic homeostasis, AMPK[125,126], which modifies

723   transcription of GC-responsive genes in a tissue- and promoter-specific manner upon

724   phosphorylation of GR's N-terminal domain[127].

725   Furthermore, biologically relevant bile acid derivatives with high affinity for the LBP of

726   oxosteroid receptors can be generated by specific modifications of the cholesterol core. This has

727   been recently demonstrated with the discovery of the LCA derivative, 3-oxo-D^{4,6}-LCA, which

728   potently and selectively binds AR and antagonizes its transcriptional activity, thus limiting prostate

729   cancer growth and metastasis[122]. This finding highlights the potential for designing bile acid-based

730   modulators of steroid receptor activity. Docking experiments indicate that the LCA isomer would

731   bind in the opposite orientation as endogenous AR ligands such as dihydrotestosterone. A few

732   conservative replacements in the E site between AR and other oxosteroid receptors are likely

733   responsible for this unique specificity of 3-oxo-D^{4,6}-LCA. For instance, the residue topologically

734   equivalent to Tyr735 in the GR is a phenylalanine in the AR. This residue is important for GR

735   transactivation, which is reduced by 30% in the Tyr735Phe mutant[128]. Our docking experiments

736   of 3-oxo-D^{4,6}-LCA on GR-LBP show that it behaves similarly to TauroCA (Fig. S2H and I),

737   binding mainly outside the internal pocket.

738   Despite the extraordinary success of drugs that target the internal ligand-binding pockets

739   of several nuclear receptors (e.g., antiandrogens for prostate cancer treatment, synthetic

740   glucocorticoids for treating asthma and other inflammatory conditions), the rapid emergence of

741   resistance and the significant side effects of these LBP-directed drugs has fueled the search for

742   new NR antagonists with alternative mechanisms of action[18]. Solvent-exposed binding pockets on

743   the surface of the LBD modules are attractive alternative targets for pharmacological intervention.

744   Our current results offer a compelling rationale for developing new GCs with reduced side effects

745   by exploiting the biochemical and biophysical properties of bile acids, including their

746   biocompatibility. This approach opens avenues for designing more selective and physiologically

747   compatible modulators of GR activity. Previous observation that a synthetic GC, tailored for

748   binding to the LBP, also binds tightly to the SF-3 pocket of GR-LBD[84] and the proven

749   pharmacological relevance of TauroCA in a model of ataxia[75] demonstrate both the feasibility and

750   the potential clinical relevance of this approach.

751

752   **MATERIAL AND METHODS**

753   **Bioinformatics analyses**

754   PDB entries 1M2Z, 7YXO and 4UDD were used as templates to run Fpocket, PockDrug and

755   CavitySpace algorithms, respectively, using the standard parameters[76–78]. Analog screenings were

756   performed using fingerprint (FP) similarity and substructure searches in the Zinc15 [129] and

757   DrugBank databases[130]. The FP search with the Erlwood FP similarity node used Morgan

758   Fingerprints with radii of 2 and 1024 bits. The substructure search was based on SMARTS

759   patterns. For the FP similarity search, we applied a similarity cut-off of 0.6. AutoDock Vina[131] and

760   Glide SP docking algorithms (www.schrodinger.com/platform/products/glide/) were used to

761   identify potential docking conformations and affinities of selected compounds (Table S4) with

762   monomeric and dimeric GR-LBD structures using PDB 4UDD and 9HDF. Prior to docking,

763   receptor and ligand molecules were parametrized by adding hydrogen atoms, removing water

764   molecules, and computing partial atomic charges. For AutoDock experiments, an exhaustiveness

765   parameter of 20 was applied to ensure thorough conformational sampling. The number of docking

766   runs and the energy range values were set to 10 and 5 kcal/mol, respectively, to promote diversity

767   in binding poses and capture a wide range of energetically favorable interactions for each ligand.

768 AlphaFold3 structure predictions: Model generation with AlphaFold3

769 (https://alphafoldserver.com/) was performed using 20 randomly generated seeds. GR-LBD

770 sequence was used along with different combinations of two ligands: corticosterone (C0R) and

771 taurocholic acid (TCH), employing ccd codes to ensure the proper chirality of the compounds

772 during the AF3 execution. The ranking scores obtained for all models were consistently over 0.8.

773 Calculation of binding energies: Binding energies were calculated using the pyDock energy

774 scoring function, which uses an adapted version of the pyDock scoring function, originally

775 developed for protein–protein interactions, to evaluate protein-ligand energetic profiles, including

776 the electrostatic, van der Waals, and desolvation terms. This scoring function was successfully

777 used in the 7th CAPRI edition[132]. The structural data of the ligands was processed with

778 AmberTools23 (www.ambermd.org/) to generate the required ligand parameters. First, the net

779 charges of the ligands were extracted from the PDB data and used for assigning partial charges.

780 The AM1-BCC method[133] was then used to assign partial charges to the ligands based on the net

781 charges. Once the ligand parameters were established, pyDock was used to calculate the binding

782 energy, allowing us to compare the energetic profiles across the different models and binding sites.

783 Docking results were visualized and analyzed with PyMOL (www.pymol.org/), which was also

784 used to prepare all structure figures.

785 **Surface plasmon resonance (SPR) assays**

786 SPR analyses were performed at 25 °C in a BIAcore T200 instrument (GE Healthcare). Highly

787 purified, Dex-bound recombinant WT ancGR2-LBD was diluted in 10 mM sodium acetate, pH

788 5.0, and directly immobilized on CM5 chips (GE Healthcare) by amine coupling at a density of

789 100 RUs for protein-protein interaction experiments, or 7000 RUs for protein-small molecule

790 interaction experiments. As a reference, one of the channels was also amine-activated and blocked

791 in the absence of protein. The running buffer was 20 mM HEPES, pH 7.2, 200 mM NaCl, 1 mM

792 DTT, 3.3% glycerol, 0.05% Tween 20. For protein-protein interaction experiments, a constant

793 concentration of 1 mM CHAPS / BOG or 40 µM of LCA was kept throughout the experiments.

794 Sensorgrams were analyzed with the BIAcore T200 Evaluation software 3.0 using the results of

795 experiments conducted with running buffer alone as baseline and fitted according to the Langmuir

796 1:1 and multisite models.

797 **Cell lines and plasmids**

798 GFP-tagged variants of mouse GR (WT, P481R and W718A) used for RNAseq and N&B

799 experiments were generated with the QuikChange II XL Site-Directed Mutagenesis Kit

800 (Stratagene) and stably integrated into the GT-Rosa26 locus via CRISPR/Cas9 homology-directed

801 repair with puromycin selection and fluorescent-activated cell sorting.

802 pHalo-H2B used for SMT experiments was generated by polymerase chain reaction (PCR)

803 amplification of the H2B coding region from an H2B-GFP template and cloned into a pFC14A

804 backbone (Promega, Madison, WI) to fuse the HaloTag to the C terminus of H2B[134]. 3134 GR KO

805 cells expressing GFP-mGR were used to generate the Halo-mGR expressing cell line by replacing

806 the tag using site-directed mutagenesis PCR.

807 Mammary adenocarcinoma 3134-derived GR knock-out (GR-KO) cells expressing GFP-

808 tagged mouse GR variants were grown in Dulbecco's modified Eagle's medium (DMEM,

809 Invitrogen) supplemented with 5 µg/ml tetracycline (Sigma), 10% fetal bovine serum (FBS,

810 Sigma), sodium pyruvate, non-essential amino acids, and 2 mM L-glutamine. Cells were

811 maintained in a humidifier at 37 °C. The FBS-supplemented medium was replaced with medium

812 supplemented with charcoal/dextran-treated FBS to remove GCs from cells for 24 h prior to

813 hormone treatment.

814 The Halo-GR cell line was generated by CRISPR/Cas9 targeted insertion of a Halo tag into

815 the N terminus of the GR gene at its endogenous locus in the mammary adenocarcinoma 3134-

816 derived cells. Treatment with IPTG induces expression of shNIPBL in these parental cells.

817 However, under the normal culturing conditions used in this study they have normal NIPBL levels

818 and GR-regulated gene responses[104].

819 **Translocation assays**

820 Prior to imaging, cells expressing GFP-GR were plated in 384-well plates (Matrical) at a density

821 of 10,000 cells per well in DMEM medium containing 10% charcoal stripped serum (Hyclone,

822 Logan, UT). Cells were activated with 100 nM Cort and treated with various concentrations of

823 LCA or TauroCA for 2 h. After treatment, cells were fixed with 4% paraformaldehyde in PBS for

824 10 min and washed three times with PBS. Cells were further stained with DAPI (4′,6-diamidino-

825 2-phenylindole, SC-3598, ChemCruz) dissolved in PBS (5 µg/ml) for 10 min, washed three times

826 with PBS, and either imaged immediately or kept in PBS at 4 °C for later imaging.

827 A Yokogawa CV7000S high-throughput dual spinning disk confocal microscope was used

828 for fully automated collection of images. Images were acquired with a 40X Olympus Plan

829 ApoChromat air objective (NA 0.9) and two sCMOS cameras (2560 × 2160 pixels) using camera

830 binning of 2×2 (Pixel size 325 nm). A single imaging plane was used and the 2×2 binning allowed

831 us to reduce the size of the files. Samples were imaged using 405 nm, 488 nm, and 561 nm

832 excitation lasers and a fixed 405/488/561/640 nm dichroic mirror on the excitation side. On the

833 emission side, the emitted light was split by a fixed 561 nm emission dichroic mirror. Specifically,

834 emitted light with wavelengths below 561 nm was reflected by the emission dichroic mirror at a

835 90-degree angle to the camera switchable 445/45 or 525/50 nm emission bandpass filters mounted

836 on a filter wheel (Camera #1). Emitted light with wavelengths above 561 nm passed through the

837 mirror and to the other camera with switchable 600/37 or 676/29 nm emission bandpass filters

838   mounted on another filter wheel (Camera #2). Camera #1 and Camera #2 were positioned

839   perpendicular to each other. DAPI (Ex. 405 nm—Em 445/45 nm) and GFP signals (Ex. 488 nm—

840   Em. 525/50 nm) were always acquired in separate exposures. Additional images were taken on a

841   PerkinElmer Opera QEHS High-Content Screening platform (Waltham, MA). This system

842   employed 40× water-immersion objective lens, a laser illuminated dual Nipkow spinning disk, and

843   cooled charge-coupled device cameras to digitally capture high-resolution confocal fluorescence

844   micrographs (323 nm pixel size with 2×2 camera pixel binning). On average, eight fields per well

845   were imaged using a single imaging plane.

846   **Single molecule tracking (SMT)**

847   <u>Microscopy:</u> All SMT experiments were performed on a custom-built, three-color highly inclined

848   laminated optical (HILO) sheet in the LRBGE Optical Microscopy Core at the National Cancer

849   Institute (NCI), National Institutes of Health (NIH). This system contains a 100x 1.49NA TIRF

850   objective (Olympus Scientific Solutions, Waltham, MA), three lasers (488, 561 and 647 nm,

851   Coherent, Inc., Santa Clara, CA), and a stage-top incubator with CO_2 control (Okolab, Pozzuoli

852   NA). The emitted light passes through a quad-band dichroic (ZT405/488/561/647, Chroma,

853   Bellows Falls, VT) and two long-pass filters (T588lpxr, T660lpxr), and is finally separated by

854   emission filters (525/50, 609/58, 736/128; Semrock) before being detected simultaneously by three

855   EMCCD cameras (Photometrics, Tucson, AZ). The pixel size for this system is 144 nm. For each

856   cell, 600 frames were collected with 10 ms exposures and 200 ms intervals with a laser power of

857   1.3 mW at the objective.

858   <u>Tracking:</u> Tracking was performed using TrackRecord. Each movie was filtered with a band-pass

859   filter and the nucleus was identified from a temporal projection of the movie. Particles detection

860   was performed using an intensity threshold where >95% of detected particles have a signal-to-

861 noise ratio ≥ 1.5. Particles were connected to form tracks using a nearest-neighbor algorithm with

862 the following parameters: maximum jump = 4 pixels (576 nm), gaps to close = 1 frame, shortest

863 track = 2 frames.

864 <u>Dwell time calculation and power-law fit:</u> Histone H2B was used to calculate the parameters of

865 bound molecules as described in[100]. Following the published procedure herein, the photobleaching

866 rate k_{PB} was calculated by fitting the H2B survival distribution to a triple-exponential function.

867 Dwell time distributions of bound GR WT and GR[tetra] molecules were corrected for

868 photobleaching by dividing the respective raw survival distributions by the exponential

869 photobleaching component:

870 $$S^{corrected}(t) = \frac{S^{raw}(t)}{e^{-k_{PB}\cdot t}}$$

871 The resulting survival distribution was then fit to double-exponential and power-law models, and

872 a Bayesian information criterion was used to determine the best model fit as described[100].

873 **N&B experiments**

874 Quantitative fluorescence microscopy images were taken at the CCR, LRBGE Optical Microscopy

875 Core facility (Bethesda, MD) using LSM 780 laser scanning microscopes (Carl Zeiss, Inc.),

876 equipped with an environmental chamber. Cells were excited with a multi-line Argon laser tuned

877 at 488 nm and imaged for 20-120 min after hormone addition using a 63× oil immersion objective

878 (NA = 1.4). Fluorescence was detected with a GaAsP detector in photon-counting mode, using

879 491-589 nm filtering,

880 N&B measurements were done as previously described[13,99]. For each studied cell, a single-

881 plane stack of 120 images (256 × 256 pixels) was taken with a pixel size of 80 nm and pixel dwell

882 times of 6.27 µs in the LSM 780 scope. In all stacks, we discarded the first 5 images to reduce the

883 effect of photobleaching. The frame time under these conditions is 0.97 s, which guarantees

884   independent sampling of molecules according to previously reported fluorescence correlation

885   spectroscopy (FCS) measurements[135]. Each stack was further analyzed using the N&B routine of

886   the SimFCS 2.0 software (Global Dynamics), in which the average fluorescence intensity (<I>)

887   and its variance ($\sigma 2$) at each pixel of an image are determined from the intensity values obtained

888   at the given pixel along the image stack. The apparent brightness (B) is calculated as the ratio of

889    $\sigma 2$ to <I> while the apparent number of moving particles (N) corresponds to the ratio of <I> to

890   B[136]. We used the SimFCS 2.0 software to classify pixels as occurring in the nucleus or the MMTV

891   array according to their intensity values[99].

892   Cells were selected for analysis following these criteria: (i) in the case of stimulated cells,

893   an accumulation of signal at the array must be visible, (ii) the average apparent number of

894   molecules (N) in the nuclear compartment must have a range of 3–30 units in all cases, (iii) no

895   saturation of the detector at any pixel (N < 60), and (iv) bleaching cannot exceed 5–10%. In

896   previous work it was demonstrated that B is equal to the real brightness ε of the particles plus

897   one[136]. Therefore, ε at every pixel of the images can be easily extracted from B values. Importantly,

898   this analysis only provides information regarding the moving or fluctuating fluorescent molecules

899   since fixed molecules (relative to our frame time) will give B values equal to 1. The

900   oligomerization state is obtained by comparing the fluorescence of full-length GR to that of a

901   constitutively monomeric GR variant, N525*. The experiments were independently repeated at

902   least two times for each treatment/condition.

Expression analysis of GR target genes by RT-qPCR

904   For time-course experiments and qPCR, GFP-GR and endogenous GR expressing cells were left

905   untreated or treated with 100 nM of Cort for 0.5, 1, 2 or 3 h prior RNA isolation, in the presence

906   or absence of bile acids at different concentrations. RNA was isolated using the PureLink RNA kit

907   (Thermo #12183018 A; Thermo Fisher Scientific) and cDNA reactions were performed with the

908   NEB Protoscript II kit (#E6560S) following the manufacturers' instructions. RT-qPCRs were

909   performed with iQ SYBR Green Supermix (Biorad # 1708880) in a Biorad CFX96 machine with

910   duplicate wells for each sample. The following primers were used to amplify *Per1* (5'-

911   CTTCTGGCAATGGCAAGGACTC-3'; 5'-CAGCATCATGCCATCATACACAC-3'), *Sgk1*

912   (5'-GAAACAGAGAAGGATGGGCCTGAAC-3'; 5'- GATCTCAGCTCCAGCACCACCAC-

913   3'), *Arl4d* (5'-AAAAGGAATATTTAGAAGGGTAGGGTGC-3'; 5'- GCCATTTCAGTCAA-

914   GTGGTTCCC-3'), *Tsc22d3* (5'- ACATGATGGTGGCATGAAGA-3'; 5'- TCTTCTCAAG-

915   CAGCTCACGA-3'), *Nr3c1* (5'-GACTTCCTTGGGGGCTATGAA-3'; 5'-

916   AACAGCAAAGTGCTGACTTAC-3'), (*β-actin* (5'- GCTGGAAAAGAGCCTCAGGGC-3'; 5'-

917   CGCATCCTC-TTCCTCCCTGGAG-3') and *18-S* (5'-GCCCGAAGCGTTTACTTTGA-3'; 5'-

918   TCCATTATTCCTAGCTGCGGTATC-3') genes. Results were normalized to either *β-actin* or

919   *18-S* expression levels, and each sample was quantified in triplicate. GraphPad Prism 8.0 software

920   was used to perform statistical analyses using one-way ANOVA followed by Tukey's post-hoc

921   test to compare group means.

922   **Total RNA collection and sequencing**

923   RNA was isolated using the PureLink RNA kit following the manufacturer's instructions. We

924   collected three biological replicates of each condition and assessed sample quality using the

925   Agilent Bioanalyzer. Strand-specific sequencing libraries were generated from rRNA-depleted

926   (Illumina RS-122-2301) total-RNA samples, using Illumina Stranded Total RNA

927   (Illumina20020596) according to the manufacturer's instructions. Raw reads were demultiplexed

928   into Fastq format allowing up to one mismatch using Illumina Bcl2fastq v2.17. Reads of the

929   samples were trimmed for adapters and low-quality bases using Cutadapt 1.18. RNA-seq

930   alignment to the mouse mm10 genome was performed with STAR[137]. DESEQ2[138] was used to

931   normalize the data by read depth, identify differentially expressed genes for each form of GR

932   (Cort/vehicle), and calculate log2 fold changes (FC) and false discovery rates (FDR) for each gene.

REFERENCES

1. Evans, R.M., and Mangelsdorf, D.J. (2014). Nuclear receptors, RXR, and the big bang. Cell *157*, 255–266. https://doi.org/10.1016/j.cell.2014.03.012.

2. Burris, T.P., de Vera, I.M.S., Cote, I., Flaveny, C.A., Wanninayake, U.S., Chatterjee, A., Walker, J.K., Steinauer, N., Zhang, J., Coons, L.A., et al. (2023). International union of basic and clinical pharmacology CXIII: Nuclear receptor superfamily—Update 2023. Pharmacol. Rev. *75*, 1233–1318. https://doi.org/10.1124/pharmrev.121.000436.

3. Font-Díaz, J., Jiménez-Panizo, A., Caelles, C., Vivanco, M. d. M., Pérez, P., Aranda, A., Estébanez-Perpiñá, E., Castrillo, A., Ricote, M., and Valledor, A.F. (2021). Nuclear receptors: Lipid and hormone sensors with essential roles in the control of cancer development. Semin. Cancer Biol. *73*, 58–75. https://doi.org/10.1016/j.semcancer.2020.12.007.

4. Kadmiel, M., and Cidlowski, J.A. (2013). Glucocorticoid receptor signaling in health and disease. Trends Pharmacol. Sci. *34*, 518–530. https://doi.org/10.1016/j.tips.2013.07.003.

5. Rhen, T., and Cidlowski, J.A. (2005). Antiinflammatory action of glucocorticoids — New mechanisms for old drugs. N. Engl. J. Med. *353*, 1711–1723. https://doi.org/10.1056/NEJMra050541.

6. Sevilla, L.M., Jiménez-Panizo, A., Alegre-Martí, A., Estébanez-Perpiñá, E., Caelles, C., and Pérez, P. (2021). Glucocorticoid resistance: interference between the glucocorticoid receptor and the mapk signalling pathways. Int. J. Mol. Sci. *22*. https://doi.org/10.3390/ijms221810049.

7. Syed, A.P., Greulich, F., Ansari, S.A., and Uhlenhaut, N.H. (2020). Anti-inflammatory glucocorticoid action: Genomic insights and emerging concepts. Curr. Opin. Pharmacol. *53*, 35–44. https://doi.org/10.1016/j.coph.2020.03.003.

957   8.   Clarisse, D., Van Moortel, L., Van Leene, C., Gevaert, K., and De Bosscher, K. (2024).

958   Glucocorticoid receptor signaling: intricacies and therapeutic opportunities. Trends

959   Biochem. Sci. *49*, 431–444. https://doi.org/10.1016/j.tibs.2024.01.012.

960   9.   Fadel, L., Dacic, M., Fonda, V., Sokolsky, B.A., Quagliarini, F., Rogatsky, I., and

961   Uhlenhaut, N.H. (2023). Modulating glucocorticoid receptor actions in physiology and

962   pathology: Insights from coregulators. Pharmacol. Ther. *251*, 108531.

963   https://doi.org/10.1016/j.pharmthera.2023.108531.

964   10. Bledsoe, R.K., Montana, V.G., Stanley, T.B., Delves, C.J., Apolito, C.J., McKee, D.D.,

965   Consler, T.G., Parks, D.J., Stewart, E.L., Willson, T.M., et al. (2002). Crystal structure of

966   the glucocorticoid receptor ligand binding domain reveals a novel mode of receptor

967   dimerization and coactivator recognition. Cell *110*, 93–105.

968   https://doi.org/10.1016/S0092-8674(02)00817-6.

969   11. Kauppi, B., Jakob, C., Färnegårdh, M., Yang, J., Ahola, H., Alarcon, M., Calles, K.,

970   Engström, O., Harlan, J., Muchmore, S., et al. (2003). The three-dimensional structures of

971   antagonistic and agonistic forms of the glucocorticoid receptor ligand-binding domain. J.

972   Biol. Chem. *278*, 22748–22754. https://doi.org/10.1074/jbc.M212711200.

973   12. Bruno, N.E., Nwachukwu, J.C., Srinivasan, S., Nettles, C.C., Izard, T., Jin, Z., Nowak, J.,

974   Cameron, M.D., Boregowda, S. V, Phinney, D.G., et al. (2021). Chemical systems biology

975   reveals mechanisms of glucocorticoid receptor signaling. Nat. Chem. Biol. *17*, 307–316.

976   https://doi.org/10.1038/s41589-020-00719-w.

977   13. Jiménez-Panizo, A., Alegre-Martí, A., Tettey, T.T., Fettweis, G., Abella, M., Antón, R.,

978   Johnson, T.A., Kim, S., Schiltz, R.L., Núñez-Barrios, I., et al. (2022). The multivalency of

979   the glucocorticoid receptor ligand-binding domain explains its manifold physiological

980   activities. Nucleic Acids Res. *50*, 13063–13082. https://doi.org/10.1093/nar/gkac1119.

981 14. Wang, Y., Chirgadze, N.Y., Briggs, S.L., Khan, S., Jensen, E. V., and Burris, T.P. (2006).

982   A second binding site for hydroxytamoxifen within the coactivator-binding groove of

983   estrogen receptor β. Proc. Natl. Acad. Sci. *103*, 9908–9911.

984   https://doi.org/10.1073/pnas.0510596103.

985 15. Estébanez-Perpiñá, E., Arnold, L.A., Jouravel, N., Togashi, M., Blethrow, J., Mar, E.,

986   Nguyen, P., Phillips, K.J., Baxter, J.D., Webb, P., et al. (2007). Structural insight into the

987   mode of action of a direct inhibitor of coregulator binding to the thyroid hormone

988   receptor. Mol. Endocrinol. *21*, 2919–2928. https://doi.org/10.1210/me.2007-0174.

989 16. Estébanez-Perpiñá, E., Arnold, L.A., Nguyen, P., Rodrigues, E.D., Mar, E., Bateman, R.,

990   Pallai, P., Shokat, K.M., Baxter, J.D., Guy, R.K., et al. (2007). A surface on the androgen

991   receptor that allosterically regulates coactivator binding. Proc. Natl. Acad. Sci. *104*,

992   16074–16079. https://doi.org/10.1073/pnas.0708036104.

993 17. Belorusova, A.Y., Eberhardt, J., Potier, N., Stote, R.H., Dejaegere, A., and Rochel, N.

994   (2014). Structural insights into the molecular mechanism of Vitamin D receptor activation

995   by lithocholic acid involving a new mode of ligand recognition. J. Med. Chem. *57*, 4710–

996   4719. https://doi.org/10.1021/jm5002524.

997 18. Gallastegui, N., and Estébanez-Perpiñá, E. (2015). Thinking outside the box: Alternative

998   binding sites in the ligand binding domain of nuclear receptors. In Nuclear Receptors:

999   From Structure to the Clinic, I. J. McEwan and R. Kumar, eds. (Springer International

1000   Publishing), pp. 179–203. https://doi.org/10.1007/978-3-319-18729-7_10.

1001 19. Sladek, F.M. (2011). What are nuclear receptor ligands? Mol. Cell. Endocrinol. *334*, 3–13.

1002   https://doi.org/10.1016/j.mce.2010.06.018.

1003 20. Jensen, E. V., and Khan, S.A. (2004). A two-site model for antiestrogen action. Mech.

1004   Ageing Dev. *125*, 679–682. https://doi.org/10.1016/j.mad.2004.08.006.

1005   21.   van Hoorn, W.P. (2002). Identification of a second binding site in the estrogen receptor. J.

1006   Med. Chem. *45*, 584–589. https://doi.org/10.1021/jm0109661.

1007   22.   Heldring, N., Nilsson, M., Buehrer, B., Treuter, E., and Gustafsson, J.-Å. (2004).

1008   Identification of tamoxifen-induced coregulator interaction surfaces within the ligand-

1009   binding domain of estrogen receptors. Mol. Cell. Biol. *24*, 3445–3459.

1010   https://doi.org/10.1128/MCB.24.8.3445-3459.2004.

1011   23.   Kong, E.H., Heldring, N., Gustafsson, J.-Å., Treuter, E., Hubbard, R.E., and Pike, A.C.W.

1012   (2005). Delineation of a unique protein–protein interaction site on the surface of the

1013   estrogen receptor. Proc. Natl. Acad. Sci. *102*, 3593–3598.

1014   https://doi.org/10.1073/pnas.0407189102.

1015   24.   Kojetin, D.J., Burris, T.P., Jensen, E. V., and Khan, S.A. (2008). Implications of the

1016   binding of tamoxifen to the coactivator recognition site of the estrogen receptor. Endocr.

1017   Relat. Cancer *15*, 851–870. https://doi.org/10.1677/ERC-07-0281.

1018   25.   Howell, A., and Howell, S.J. (2023). Tamoxifen evolution. Br. J. Cancer *128*, 421–425.

1019   https://doi.org/10.1038/s41416-023-02158-5.

1020   26.   De Leon, J.T., Iwai, A., Feau, C., Garcia, Y., Balsiger, H.A., Storer, C.L., Suro, R.M.,

1021   Garza, K.M., Lee, S., Sang Kim, Y., et al. (2011). Targeting the regulation of androgen

1022   receptor signaling by the heat shock protein 90 cochaperone FKBP52 in prostate cancer

1023   cells. Proc. Natl. Acad. Sci. *108*, 11878–11883. https://doi.org/10.1073/pnas.1105160108.

1024   27.   Jehle, K., Cato, L., Neeb, A., Muhle-Goll, C., Jung, N., Smith, E.W., Buzon, V., Carbó,

1025   L.R., Estébanez-Perpiñá, E., Schmitz, K., et al. (2014). Coregulator control of androgen

1026   receptor action by a novel nuclear receptor-binding motif. J. Biol. Chem. *289*, 8839–8851.

1027   https://doi.org/10.1074/jbc.M113.534859.

1028   28.   Noddings, C.M., Wang, R.Y.-R., Johnson, J.L., and Agard, D.A. (2022). Structure of

1029   Hsp90–p23–GR reveals the Hsp90 client-remodelling mechanism. Nature *601*, 465–469.

1030   https://doi.org/10.1038/s41586-021-04236-1.

1031   29.   Buzón, V., Carbó, L.R., Estruch, S.B., Fletterick, R.J., and Estébanez-Perpiñá, E. (2012).

1032   A conserved surface on the ligand binding domain of nuclear receptors for allosteric

1033   control. Mol. Cell. Endocrinol. *348*, 394–402. https://doi.org/10.1016/j.mce.2011.08.012.

1034   30.   Chandra, V., Huang, P., Potluri, N., Wu, D., Kim, Y., and Rastinejad, F. (2013).

1035   Multidomain integration in the structure of the HNF-4α nuclear receptor complex. Nature

1036   *495*, 394–398. https://doi.org/10.1038/nature11966.

1037   31.   Souza, P.C.T., Puhl, A.C., Martínez, L., Aparício, R., Nascimento, A.S., Figueira, A.C.M.,

1038   Nguyen, P., Webb, P., Skaf, M.., and Polikarpov, I. (2014). Identification of a new

1039   hormone-binding site on the surface of thyroid hormone receptor. Mol. Endocrinol. *28*,

1040   534–545. https://doi.org/10.1210/me.2013-1359.

1041   32.   Zhan, Y., Chen, Y., Zhang, Q., Zhuang, J., Tian, M., Chen, H., Zhang, L., Zhang, H., He,

1042   J., Wang, W., et al. (2012). The orphan nuclear receptor Nur77 regulates LKB1

1043   localization and activates AMPK. Nat. Chem. Biol. *8*, 897–904.

1044   https://doi.org/10.1038/nchembio.1069.

1045   33.   Chiang, J.Y.L., and Ferrell, J.M. (2019). Bile acids as metabolic regulators and nutrient

1046   sensors. Annu. Rev. Nutr. *39*, 175–200. https://doi.org/10.1146/annurev-nutr-082018-

1047   124344.

1048   34.   Nguyen, J.T., Shaw, R.P.H., and Anakk, S. (2022). Bile Acids - A peek into their history

1049   and signaling. Endocrinology *163*, 1–17. https://doi.org/10.1210/endocr/bqac155.

1050   35.   Mohanty, I., Allaband, C., Mannochio-Russo, H., El Abiead, Y., Hagey, L.R., Knight, R.,

1051   and Dorrestein, P.C. (2024). The changing metabolic landscape of bile acids – keys to

1052   metabolism and immune regulation. Nat. Rev. Gastroenterol. Hepatol. *21*, 493–516.

1053   https://doi.org/10.1038/s41575-024-00914-3.

1054   36.   Nishida, T., Gatmaitan, Z., Che, M., and Arias, I.M. (1991). Rat liver canalicular

1055   membrane vesicles contain an ATP-dependent bile acid transport system. Proc. Natl.

1056   Acad. Sci. *88*, 6590–6594. https://doi.org/10.1073/pnas.88.15.6590.

1057   37.   Lefebvre, P., Cariou, B., Lien, F., Kuipers, F., and Staels, B. (2009). Role of bile acids and

1058   bile acid receptors in metabolic regulation. Physiol. Rev. *89*, 147–191.

1059   https://doi.org/10.1152/physrev.00010.2008.

1060   38.   Fu, D., Wakabayashi, Y., Lippincott-Schwartz, J., and Arias, I.M. (2011). Bile acid

1061   stimulates hepatocyte polarization through a cAMP-Epac-MEK-LKB1- AMPK pathway.

1062   Proc. Natl. Acad. Sci. *108*, 1403–1408. https://doi.org/10.1073/pnas.1018376108.

1063   39.   Belkaid, Y., and Hand, T.W. (2014). Role of the microbiota in immunity and

1064   inflammation. Cell *157*, 121–141. https://doi.org/10.1016/j.cell.2014.03.011.

1065   40.   Lee, J.M., Wagner, M., Xiao, R., Kim, K.H., Feng, D., Lazar, M.A., and Moore, D.D.

1066   (2014). Nutrient-sensing nuclear receptors coordinate autophagy. Nature *516*, 112–115.

1067   https://doi.org/10.1038/nature13961.

1068   41.   Sinclair, D.A. (2024). A bile acid could explain how calorie restriction slows ageing.

1069   Nature, 1–2. https://doi.org/10.1038/d41586-024-04062-1.

1070   42.   Hylemon, P.B., Zhou, H., Pandak, W.M., Ren, S., Gil, G., and Dent, P. (2009). Bile acids

1071   as regulatory molecules. J. Lipid Res. *50*, 1509–1520.

1072   https://doi.org/10.1194/jlr.R900007-JLR200.

1073   43.   Chen, M.L., Takeda, K., and Sundrud, M.S. (2019). Emerging roles of bile acids in

1074   mucosal immunity and inflammation. Mucosal Immunol. *12*, 851–861.

1075   https://doi.org/10.1038/s41385-019-0162-4.

1076   44.   Claudel, T., and Trauner, M. (2010). Bile acids and their receptors. In Signaling Pathways

1077   in Liver Diseases (Springer Berlin Heidelberg), pp. 317–332. https://doi.org/10.1007/978-

1078   3-642-00150-5_21.

1079   45.   Simon, F.R., and Arias, I.M. (1973). Alteration of bile canalicular enzymes in cholestasis.

1080   A possible cause of bile secretory failure. J. Clin. Invest. *52*, 765–775.

1081   https://doi.org/10.1172/JCI107239.

1082   46.   van Mil, S.W.C., Milona, A., Dixon, P.H., Mullenbach, R., Geenes, V.L., Chambers, J.,

1083   Shevchuk, V., Moore, G.E., Lammert, F., Glantz, A.G., et al. (2007). Functional variants

1084   of the central bile acid sensor FXR identified in intrahepatic cholestasis of pregnancy.

1085   Gastroenterology *133*, 507–516. https://doi.org/10.1053/j.gastro.2007.05.015.

1086   47.   van Schaik, F.D.M., Gadaleta, R.M., Schaap, F.G., van Mil, S.W.C., Siersema, P.D.,

1087   Oldenburg, B., and van Erpecum, K.J. (2012). Pharmacological activation of the bile acid

1088   nuclear farnesoid X receptor is feasible in patients with quiescent crohn's colitis. PLoS

1089   One *7*, e49706. https://doi.org/10.1371/journal.pone.0049706.

1090   48.   Anakk, S., Bhosale, M., Schmidt, V.A., Johnson, R.L., Finegold, M.J., and Moore, D.D.

1091   (2013). Bile acids activate YAP to promote liver carcinogenesis. Cell Rep. *5*, 1060–1069.

1092   https://doi.org/10.1016/j.celrep.2013.10.030.

1093   49.   Desai, M.S., Mathur, B., Eblimit, Z., Vasquez, H., Taegtmeyer, H., Karpen, S.J., Penny,

1094   D.J., Moore, D.D., and Anakk, S. (2017). Bile acid excess induces cardiomyopathy and

1095   metabolic dysfunctions in the heart. Hepatology *65*, 189–201.

1096   https://doi.org/10.1002/hep.28890.

1097   50.   Kim, K.H., Choi, J.M., Li, F., Arizpe, A., Wooton-Kee, C.R., Anakk, S., Jung, S.Y.,

1098   Finegold, M.J., and Moore, D.D. (2018). Xenobiotic nuclear receptor signaling determines

1099   molecular pathogenesis of progressive familial intrahepatic cholestasis. Endocrinology

1100   *159*, 2435–2446. https://doi.org/10.1210/en.2018-00110.

1101 51. Zhou, W., VanDuyne, P., Zhang, C., Liu, Y., Riessen, R., Barragan, M., Rowitz, B.M.,

1102   Teran-Garcia, M., Boppart, S.A., and Anakk, S. (2023). Pathological bile acid

1103   concentrations in chronic cholestasis cause adipose mitochondrial defects. JHEP Reports

1104   *5*, 100714. https://doi.org/10.1016/j.jhepr.2023.100714.

1105 52. Patton, M.E., Kelekar, S., Taylor, L.J., Dean, A.E., Zuo, Q., Thakare, R.N., Lee, S.H.,

1106   Gentry, E., Panitchpakdi, M., Dorrestein, P., et al. (2024). Sex differences in bile acid

1107   homeostasis and excretion underlie the disparity in liver cancer incidence between males

1108   and females, https://doi.org/10.7554/eLife.96783.1 https://doi.org/10.7554/eLife.96783.1.

1109 53. Peet, D.J., Turley, S.D., Ma, W., Janowski, B.A., Lobaccaro, J.-M.A., Hammer, R.E., and

1110   Mangelsdorf, D.J. (1998). Cholesterol and bile acid metabolism are impaired in mice

1111   lacking the nuclear oxysterol receptor LXRα. Cell *93*, 693–704.

1112   https://doi.org/10.1016/S0092-8674(00)81432-4.

1113 54. Janowski, B.A., Grogan, M.J., Jones, S.A., Wisely, G.B., Kliewer, S.A., Corey, E.J., and

1114   Mangelsdorf, D.J. (1999). Structural requirements of ligands for the oxysterol liver X

1115   receptors LXRα and LXRβ. Proc. Natl. Acad. Sci. *96*, 266–271.

1116   https://doi.org/10.1073/pnas.96.1.266.

1117 55. Makishima, M., Okamoto, A.Y., Repa, J.J., Tu, H., Learned, R.M., Luk, A., Hull, M. V.,

1118   Lustig, K.D., Mangelsdorf, D.J., and Shan, B. (1999). Identification of a nuclear receptor

1119   for bile acids. Science *284*, 1362–1365. https://doi.org/10.1126/science.284.5418.1362.

1120 56. Lu, T.T., Makishima, M., Repa, J.J., Schoonjans, K., Kerr, T.A., Auwerx, J., and

1121   Mangelsdorf, D.J. (2000). Molecular basis for feedback regulation of bile acid synthesis

1122   by nuclear receptos. Mol. Cell *6*, 507–515. https://doi.org/10.1016/S1097-2765(00)00050-

1123   2.

1124 57. Pineda Torra, I., Claudel, T., Duval, C., Kosykh, V., Fruchart, J.-C., and Staels, B. (2003).

1125   Bile acids induce the expression of the human peroxisome proliferator-activated receptor

1126   α gene via activation of the farnesoid X receptor. Mol. Endocrinol. *17*, 259–272.

1127   https://doi.org/10.1210/me.2002-0120.

1128   58.   Mi, L.-Z., Devarakonda, S., Harp, J.M., Han, Q., Pellicciari, R., Willson, T.M.,

1129   Khorasanizadeh, S., and Rastinejad, F. (2003). Structural basis for bile acid binding and

1130   activation of the nuclear receptor FXR. Mol. Cell *11*, 1093–1100.

1131   https://doi.org/10.1016/S1097-2765(03)00112-6.

1132   59.   Downes, M., Verdecia, M.A., Roecker, A.J., Hughes, R., Hogenesch, J.B., Kast-

1133   Woelbern, H.R., Bowman, M.E., Ferrer, J.-L., Anisfeld, A.M., Edwards, P.A., et al.

1134   (2003). A chemical, genetic, and structural analysis of the nuclear bile acid receptor FXR.

1135   Mol. Cell *11*, 1079–1092. https://doi.org/10.1016/S1097-2765(03)00104-7.

1136   60.   Belorusova, A.Y., and Rochel, N. (2016). Structural studies of Vitamin D nuclear receptor

1137   ligand-binding properties. In Vitamins and Hormones, pp. 83–116.

1138   https://doi.org/10.1016/bs.vh.2015.10.003.

1139   61.   Belorusova, A.Y., and Rochel, N. (2024). Structural basis for ligand activity in vitamin D

1140   receptor. In Feldman and Pike' s Vitamin D (Elsevier), pp. 189–212.

1141   https://doi.org/10.1016/B978-0-323-91386-7.00027-1.

1142   62.   Staudinger, J.L., Goodwin, B., Jones, S.A., Hawkins-Brown, D., MacKenzie, K.I.,

1143   LaTour, A., Liu, Y., Klaassen, C.D., Brown, K.K., Reinhard, J., et al. (2001). The nuclear

1144   receptor PXR is a lithocholic acid sensor that protects against liver toxicity. Proc. Natl.

1145   Acad. Sci. *98*, 3369–3374. https://doi.org/10.1073/pnas.051551698.

1146   63.   Kliewer, S.A., and Willson, T.M. (2002). Regulation of xenobiotic and bile acid

1147   metabolism by the nuclear pregnane X receptor. J. Lipid Res. *43*, 359–364.

1148   https://doi.org/10.1016/S0022-2275(20)30141-3.

1149   64.   Willson, T.M., and Kliewer, S.A. (2002). PXR, CAR and drug metabolism. Nat. Rev.

1150   Drug Discov. *1*, 259–266. https://doi.org/10.1038/nrd753.

1151   65.   Suino, K., Peng, L., Reynolds, R., Li, Y., Cha, J.-Y., Repa, J.J., Kliewer, S.A., and Xu,

1152   H.E. (2004). The nuclear xenobiotic receptor CAR: Structural determinants of constitutive

1153   activation and heterodimerization. Mol. Cell *16*, 893–905.

1154   https://doi.org/10.1016/j.molcel.2004.11.036.

1155   66.   Cheung, K.C.P., Ma, J., Loiola, R.A., Chen, X., and Jia, W. (2023). Bile acid-activated

1156   receptors in innate and adaptive immunity: Targeted drugs and biological agents. Eur. J.

1157   Immunol. *53*, 1–14. https://doi.org/10.1002/eji.202250299.

1158   67.   Liu, J., Tan, Y., Cheng, H., Zhang, D., Feng, W., and Peng, C. (2022). Functions of gut

1159   microbiota metabolites, current status and future perspectives. Aging Dis. *13*, 1106–1126.

1160   https://doi.org/10.14336/AD.2022.0104.

1161   68.   Collins, S.L., Stine, J.G., Bisanz, J.E., Okafor, C.D., and Patterson, A.D. (2023). Bile

1162   acids and the gut microbiota: Metabolic interactions and impacts on disease. Nat. Rev.

1163   Microbiol. *21*, 236–247. https://doi.org/10.1038/s41579-022-00805-x.

1164   69.   Ridlon, J.M., and Gaskins, H.R. (2024). Another renaissance for bile acid gastrointestinal

1165   microbiology. Nat. Rev. Gastroenterol. Hepatol. *21*, 348–364.

1166   https://doi.org/10.1038/s41575-024-00896-2.

1167   70.   Fiorucci, S., Baldoni, M., Ricci, P., Zampella, A., Distrutti, E., and Biagioli, M. (2020).

1168   Bile acid-activated receptors and the regulation of macrophages function in metabolic

1169   disorders. Curr. Opin. Pharmacol. *53*, 45–54. https://doi.org/10.1016/j.coph.2020.04.008.

1170   71.   Lee, M.H., Nuccio, S.-P., Mohanty, I., Hagey, L.R., Dorrestein, P.C., Chu, H., and

1171   Raffatellu, M. (2024). How bile acids and the microbiota interact to shape host immunity.

1172   Nat. Rev. Immunol. *24*, 798–809. https://doi.org/10.1038/s41577-024-01057-x.

1173   72.   Wang, Y.-D., Chen, W.-D., Moore, D.D., and Huang, W. (2008). FXR: A metabolic

1174   regulator and cell protector. Cell Res. *18*, 1087–1095. https://doi.org/10.1038/cr.2008.289.

1175   73.   Chiang, J.Y.L., and Ferrell, J.M. (2020). Bile acid receptors FXR and TGR5 signaling in

1176   fatty liver diseases and therapy. Am. J. Physiol. Liver Physiol. *318*, G554–G573.

1177   https://doi.org/10.1152/ajpgi.00223.2019.

1178   74.   Takigawa, T., Miyazaki, H., Kinoshita, M., Kawarabayashi, N., Nishiyama, K., Hatsuse,

1179   K., Ono, S., Saitoh, D., Seki, S., and Yamamoto, J. (2013). Glucocorticoid receptor-

1180   dependent immunomodulatory effect of ursodeoxycholic acid on liver lymphocytes in

1181   mice. Am. J. Physiol. Liver Physiol. *305*, G427–G438.

1182   https://doi.org/10.1152/ajpgi.00205.2012.

1183   75.   Duarte-Silva, S., Da Silva, J.D., Monteiro-Fernandes, D., Costa, M.D., Neves-Carvalho,

1184   A., Raposo, M., Soares-Cunha, C., Correia, J.S., Nogueira-Goncalves, G., Fernandes,

1185   H.S., et al. (2024). Glucocorticoid receptor-dependent therapeutic efficacy of

1186   tauroursodeoxycholic acid in preclinical models of spinocerebellar ataxia type 3. J. Clin.

1187   Invest. *134*, 1–19. https://doi.org/10.1172/JCI162246.

1188   76.   Le Guilloux, V., Schmidtke, P., and Tuffery, P. (2009). Fpocket: An open source platform

1189   for ligand pocket detection. BMC Bioinformatics *10*, 168. https://doi.org/10.1186/1471-

1190   2105-10-168.

1191   77.   Borrel, A., Regad, L., Xhaard, H., Petitjean, M., and Camproux, A.-C. (2015). PockDrug:

1192   A model for predicting pocket druggability that overcomes pocket estimation

1193   uncertainties. J. Chem. Inf. Model. *55*, 882–895. https://doi.org/10.1021/ci5006004.

1194   78.   Wang, S., Lin, H., Huang, Z., He, Y., Deng, X., Xu, Y., Pei, J., and Lai, L. (2022).

1195   CavitySpace: A dpatabase of potential ligand binding sites in the human roteome.

1196   Biomolecules *12*, 967. https://doi.org/10.3390/biom12070967.

1197   79.   Nettles, K.W., Bruning, J.B., Gil, G., Nowak, J., Sharma, S.K., Hahm, J.B., Kulp, K.,

1198   Hochberg, R.B., Zhou, H., Katzenellenbogen, J.A., et al. (2008). NFκB selectivity of

1199   estrogen receptor ligands revealed by comparative crystallographic analyses. Nat. Chem.

1200   Biol. *4*, 241–247. https://doi.org/10.1038/nchembio.76.

1201   80.   Biggadike, K., Bledsoe, R.K., Coe, D.M., Cooper, T.W.J., House, D., Iannone, M.A.,

1202   Macdonald, S.J.F., Madauss, K.P., McLay, I.M., Shipley, T.J., et al. (2009). Design and x-

1203   ray crystal structures of high-potency nonsteroidal glucocorticoid agonists exploiting a

1204   novel binding site on the receptor. Proc. Natl. Acad. Sci. *106*, 18114–18119.

1205   https://doi.org/10.1073/pnas.0909125106.

1206   81.   Edman, K., Hosseini, A., Bjursell, M.K., Aagaard, A., Wissler, L., Gunnarsson, A.,

1207   Kaminski, T., Köhler, C., Bäckström, S., Jensen, T.J., et al. (2015). Ligand binding

1208   mechanism in steroid receptors: From conserved plasticity to differential evolutionary

1209   constraints. Structure *23*, 2280–2290. https://doi.org/10.1016/j.str.2015.09.012.

1210   82.   Berger, M., Rehwinkel, H., Schmees, N., Schäcke, H., Edman, K., Wissler, L., Reichel,

1211   A., and Jaroch, S. (2017). Discovery of new selective glucocorticoid receptor agonist

1212   leads. Bioorg. Med. Chem. Lett. *27*, 437–442. https://doi.org/10.1016/j.bmcl.2016.12.047.

1213   83.   Hemmerling, M., Nilsson, S., Edman, K., Eirefelt, S., Russell, W., Hendrickx, R.,

1214   Johnsson, E., Kärrman Mårdh, C., Berger, M., Rehwinkel, H., et al. (2017). Selective

1215   nonsteroidal glucocorticoid receptor modulators for the inhaled treatment of pulmonary

1216   diseases. J. Med. Chem. *60*, 8591–8605. https://doi.org/10.1021/acs.jmedchem.7b01215.

1217   84.   Carson, M.W., Luz, J.G., Suen, C., Montrose, C., Zink, R., Ruan, X., Cheng, C., Cole, H.,

1218   Adrian, M.D., Kohlman, D.T., et al. (2014). Glucocorticoid receptor modulators informed

1219   by crystallography lead to a new rationale for receptor selectivity, function, and

1220   implications for structure-based design. J. Med. Chem. *57*, 849–860.

1221   https://doi.org/10.1021/jm401616g.

1222   85.   Alegre-Martí, A., Jiménez-Panizo, A., Lafuente, A.L., Johnson, T.A., Montoya-Novoa, I.,

1223   Abella, M., Pérez, P., Fernández-Recio, J., Presman, D.M., Hager, G.L., et al. (2024). The

1224   multimerization pathway of the glucocorticoid receptor. bioRxiv, 2024.12.12.628195.

1225   https://doi.org/10.1101/2024.12.12.628195.

1226   86.   Wallace, A.D., and Cidlowski, J.A. (2001). Proteasome-mediated glucocorticoid receptor

1227   degradation restricts transcriptional signaling by glucocorticoids. J. Biol. Chem. *276*,

1228   42714–42721. https://doi.org/10.1074/jbc.M106033200.

1229   87.   Wang, X., and DeFranco, D.B. (2005). Alternative effects of the ubiquitin-proteasome

1230   pathway on glucocorticoid receptor down-regulation and transactivation are mediated by

1231   CHIP, an E3 ligase. Mol. Endocrinol. *19*, 1474–1482. https://doi.org/10.1210/me.2004-

1232   0383.

1233   88.   Gälman, C., Angelin, B., and Rudling, M. (2005). Bile acid synthesis in humans has a

1234   rapid diurnal variation that is asynchronous with cholesterol synthesis. Gastroenterology

1235   *129*, 1445–1453. https://doi.org/10.1053/j.gastro.2005.09.009.

1236   89.   Gälman, C., Angelin, B., and Rudling, M. (2011). Pronounced variation in bile acid

1237   synthesis in humans is related to gender, hypertriglyceridaemia and circulating levels of

1238   fibroblast growth factor 19. J. Intern. Med. *270*, 580–588. https://doi.org/10.1111/j.1365-

1239   2796.2011.02466.x.

1240   90.   Azer, S.A., and Hasanato, R. (2021). Use of bile acids as potential markers of liver

1241   dysfunction in humans. Medicine (Baltimore). *100*, e27464.

1242   https://doi.org/10.1097/MD.0000000000027464.

1243   91.   Fleishman, J.S., and Kumar, S. (2024). Bile acid metabolism and signaling in health and

1244   disease: Molecular mechanisms and therapeutic targets. Signal Transduct. Target. Ther. *9*,

1245   97. https://doi.org/10.1038/s41392-024-01811-6.

1246   92.   Dong, Y., Poellinger, L., Gustafsson, J.-Å., and Okret, S. (1988). Regulation of

1247   glucocorticoid receptor expression: Evidence for transcriptional and posttranslational

1248   mechanisms. Mol. Endocrinol. *2*, 1256–1264. https://doi.org/10.1210/mend-2-12-1256.

1249   93.   Ramamoorthy, S., and Cidlowski, J.A. (2013). Ligand-induced repression of the

1250   glucocorticoid receptor gene is mediated by an NCoR1 repression complex formed by

1251   long-range chromatin interactions with intragenic glucocorticoid response elements. Mol.

1252   Cell. Biol. *33*, 1711–1722. https://doi.org/10.1128/MCB.01151-12.

1253   94.   Glantschnig, C., Koenen, M., Gil-Lozano, M., Karbiener, M., Pickrahn, I., Williams-

1254   Dautovich, J., Patel, R., Cummins, C.L., Giroud, M., Hartleben, G., et al. (2019). A miR-

1255   29a-driven negative feedback loop regulates peripheral glucocorticoid receptor signaling.

1256   FASEB J. *33*, 5924–5941. https://doi.org/10.1096/fj.201801385RR.

1257   95.   Song, P., Zhang, Y., and Klaassen, C.D. (2011). Dose-response of five bile acids on serum

1258   and liver bile acid concentrations and hepatotoxicty in mice. Toxicol. Sci. *123*, 359–367.

1259   https://doi.org/10.1093/toxsci/kfr177.

1260   96.   Wagh, K., Stavreva, D.A., Upadhyaya, A., and Hager, G.L. (2023). Transcription factor

1261   dynamics: One molecule at a time, https://doi.org/10.1146/annurev-cellbio-022823-

1262   013847 https://doi.org/10.1146/annurev-cellbio-022823-013847.

1263   97.   Wagh, K., Stavreva, D.A., and Hager, G.L. (2025). Transcription dynamics and genome

1264   organization in the mammalian nucleus: Recent advances. Mol. Cell *85*, 208–224.

1265   https://doi.org/10.1016/j.molcel.2024.09.022.

1266   98.   Presman, D.M., Ogara, M.F., Stortz, M., Alvarez, L.D., Pooley, J.R., Schiltz, R.L.,

1267   Grøntved, L., Johnson, T.A., Mittelstadt, P.R., Ashwell, J.D., et al. (2014). Live cell

1268   imaging unveils multiple domain requirements for in vivo dimerization of the

1269   glucocorticoid receptor. PLoS Biol. *12*, e1001813.

1270   https://doi.org/10.1371/journal.pbio.1001813.

1271 99. Presman, D.M., Ganguly, S., Schiltz, R.L., Johnson, T.A., Karpova, T.S., and Hager, G.L.

1272   (2016). DNA binding triggers tetramerization of the glucocorticoid receptor in live cells.

1273   Proc. Natl. Acad. Sci. *113*, 8236–8241. https://doi.org/10.1073/pnas.1606774113.

1274 100. Garcia, D.A., Fettweis, G., Presman, D.M., Paakinaho, V., Jarzynski, C., Upadhyaya, A.,

1275   and Hager, G.L. (2021). Power-law behavior of transcription factor dynamics at the

1276   single-molecule level implies a continuum affinity model. Nucleic Acids Res. *49*, 6605–

1277   6620. https://doi.org/10.1093/nar/gkab072.

1278 101. Wagh, K., Stavreva, D.A., Jensen, R.A.M., Paakinaho, V., Fettweis, G., Schiltz, R.L.,

1279   Wüstner, D., Mandrup, S., Presman, D.M., Upadhyaya, A., et al. (2023). Dynamic

1280   switching of transcriptional regulators between two distinct low-mobility chromatin states.

1281   Sci. Adv. *9*, 1–19. https://doi.org/10.1126/sciadv.ade1122.

1282 102. Johnson, T.A., Fettweis, G., Wagh, K., Ceacero-Heras, D., Krishnamurthy, M., Sánchez

1283   de Medina, F., Martínez-Augustin, O., Upadhyaya, A., Hager, G.L., and Alvarez de la

1284   Rosa, D. (2024). The glucocorticoid receptor potentiates aldosterone-induced transcription

1285   by the mineralocorticoid receptor. Proc. Natl. Acad. Sci. U. S. A. *121*.

1286   https://doi.org/10.1073/pnas.2413737121.

1287 103. Garcia, D.A., Johnson, T.A., Presman, D.M., Fettweis, G., Wagh, K., Rinaldi, L.,

1288   Stavreva, D.A., Paakinaho, V., Jensen, R.A.M., Mandrup, S., et al. (2021). An

1289   intrinsically disordered region-mediated confinement state contributes to the dynamics

1290   and function of transcription factors. Mol. Cell *81*, 1484-1498.e6.

1291   https://doi.org/10.1016/j.molcel.2021.01.013.

1292 104. Fettweis, G., Wagh, K., Stavreva, D.A., Jiménez-Panizo, A., Kim, S., Lion, M., Alegre-

1294   factors form a ternary complex with NIPBL/MAU2 to localize cohesin at enhancers.

1295   bioRxiv, 2024.12.09.627537. https://doi.org/10.1101/2024.12.09.627537.

1296 105.   Stavreva, D.A., Wiench, M., John, S., Conway-Campbell, B.L., McKenna, M.A., Pooley,

1297   J.R., Johnson, T.A., Voss, T.C., Lightman, S.L., and Hager, G.L. (2009). Ultradian

1298   hormone stimulation induces glucocorticoid receptor-mediated pulses of gene

1299   transcription. Nat. Cell Biol. *11*, 1093–1102. https://doi.org/10.1038/ncb1922.

1300 106.   Presman, D.M., and Hager, G.L. (2017). More than meets the dimer: What is the

1301   quaternary structure of the glucocorticoid receptor? Transcription *8*, 32–39.

1302   https://doi.org/10.1080/21541264.2016.1249045.

1303 107.   Abrusán, G., and Marsh, J.A. (2019). Ligand binding site structure shapes folding,

1304   assembly and degradation of homomeric protein complexes. J. Mol. Biol. *431*, 3871–

1305   3888. https://doi.org/10.1016/j.jmb.2019.07.014.

1306 108.   Abrusán, G., and Foguet, C. (2023). An assessment of quaternary structure functionality in

1307   homomer protein complexes. Mol. Biol. Evol. *40*, 1–18.

1308   https://doi.org/10.1093/molbev/msad070.

1309 109.   Wang, R.Y.-R., Noddings, C.M., Kirschke, E., Myasnikov, A.G., Johnson, J.L., and

1310   Agard, D.A. (2022). Structure of Hsp90–Hsp70–Hop–GR reveals the Hsp90 client-

1311   loading mechanism. Nature *601*, 460–464. https://doi.org/10.1038/s41586-021-04252-1.

1312 110.   Noddings, C.M., Johnson, J.L., and Agard, D.A. (2023). Cryo-EM reveals how Hsp90 and

1313   FKBP immunophilins co-regulate the glucocorticoid receptor. Nat. Struct. Mol. Biol. *30*,

1314   1867–1877. https://doi.org/10.1038/s41594-023-01128-y.

1315 111.   Stavreva, D.A., Müller, W.G., Hager, G.L., Smith, C.L., and McNally, J.G. (2004). Rapid

1316   lrucocorticoid Receptor exchange at a promoter is coupled to transcription and regulated

1317   by chaperones and proteasomes. Mol. Cell. Biol. *24*, 2682–2697.

1318   https://doi.org/10.1128/MCB.24.7.2682-2697.2004.

1319   112. Seitz, T., Thoma, R., Schoch, G.A., Stihle, M., Benz, J., D'Arcy, B., Wiget, A., Ruf, A.,

1320   Hennig, M., and Sterner, R. (2010). Enhancing the stability and solubility of the

1321   glucocorticoid receptor ligand-binding domain by high-throughput library screening. J.

1322   Mol. Biol. *403*, 562–577. https://doi.org/10.1016/j.jmb.2010.08.048.

1323   113. Álvarez, L.D., Presman, D.M., and Pecci, A. (2017). Molecular dynamics simulations of

1324   the glucocorticoid receptor DNA-binding domain suggest a role of the lever-arm mobility

1325   in transcriptional output. PLoS One *12*, e0189588.

1326   https://doi.org/10.1371/journal.pone.0189588.

1327   114. Bledsoe, R.K., Madauss, K.P., Holt, J.A., Apolito, C.J., Lambert, M.H., Pearce, K.H.,

1328   Stanley, T.B., Stewart, E.L., Trump, R.P., Willson, T.M., et al. (2005). A ligand-mediated

1329   hydrogen bond network required for the activation of the mineralocorticoid receptor. J.

1330   Biol. Chem. *280*, 31283–31293. https://doi.org/10.1074/jbc.M504098200.

1331   115. Greschik, H., Flaig, R., Renaud, J.P., and Moras, D. (2004). Structural basis for the

1332   deactivation of the estrogen-related receptor γ by diethylstilbestrol or 4-hydroxytamoxifen

1333   and determinants of selectivity. J. Biol. Chem. *279*, 33639–33646.

1334   https://doi.org/10.1074/jbc.M402195200.

1335   116. Diennet, M., Shaikh, F., El Ezzy, M., Thiombane, K., Weber, S., Poupart, J., Mendoza-

1336   Sanchez, R., Gao, Z., Gleason, J., Schuetz, D.A., et al. (2023). Structural determinants of

1337   pure antiestrogenicity, https://doi.org/10.1101/2023.10.31.564979

1338   https://doi.org/10.1101/2023.10.31.564979.

1339   117. Solá, S., Amaral, J.D., Castro, R.E., Ramalho, R.M., Borralho, P.M., Kren, B.T., Tanaka,

1340   H., Steer, C.J., and Rodrigues, C.M.P. (2005). Nuclear translocation of UDCA by the

1341   glucocorticoid receptor is required to reduce TGF-β1-induced apoptosis in rat hepatocytes.

1342   Hepatology *42*, 925–934. https://doi.org/10.1002/hep.20870.

1343 118. Hofmann, A.F., and Hagey, L.R. (2008). Bile acids: Chemistry, pathochemistry, biology,

1344   pathobiology, and therapeutics. Cell. Mol. Life Sci. *65*, 2461–2483.

1345   https://doi.org/10.1007/s00018-008-7568-6.

1346 119. Mohanty, I., Mannochio-Russo, H., Schweer, J. V., El Abiead, Y., Bittremieux, W., Xing,

1347   S., Schmid, R., Zuffa, S., Vasquez, F., Muti, V.B., et al. (2024). The underappreciated

1348   diversity of bile acid modifications. Cell *187*, 1801-1818.e20.

1349   https://doi.org/10.1016/j.cell.2024.02.019.

1350 120. Guzior, D. V., Okros, M., Shivel, M., Armwald, B., Bridges, C., Fu, Y., Martin, C.,

1351   Schilmiller, A.L., Miller, W.M., Ziegler, K.M., et al. (2024). Bile salt hydrolase

1352   acyltransferase activity expands bile acid diversity. Nature *626*, 852–858.

1353   https://doi.org/10.1038/s41586-024-07017-8.

1354 121. Rimal, B., Collins, S.L., Tanes, C.E., Rocha, E.R., Granda, M.A., Solanki, S., Hoque,

1355   N.J., Gentry, E.C., Koo, I., Reilly, E.R., et al. (2024). Bile salt hydrolase catalyses

1356   formation of amine-conjugated bile acids. Nature *626*, 859–863.

1357   https://doi.org/10.1038/s41586-023-06990-w.

1358 122. Jin, W.B., Xiao, L., Jeong, M., Han, S.J., Zhang, W., Yano, H., Shi, H., Arifuzzaman, M.,

1359   Lyu, M., Wang, D., et al. (2025). Microbiota-derived bile acids antagonize the host

1360   androgen receptor and drive anti-tumor immunity. Cell *188*, 2336-2353.e38.

1361   https://doi.org/10.1016/j.cell.2025.02.029.

1362 123. Bock, P.E., Panizzi, P., and Verhamme, I.M.A. (2007). Exosites in the substrate

1363   specificity of blood coagulation reactions. J. Thromb. Haemost. *5*, 81–94.

1364   https://doi.org/10.1111/j.1538-7836.2007.02496.x.

1365 124. Baptissart, M., Vega, A., Martinot, E., Baron, S., Lobaccaro, J.M.A., and Volle, D.H.

1366   (2013). Farnesoid X receptor alpha: A molecular link between bile acids and steroid

1367   signaling? Cell. Mol. Life Sci. *70*, 4511–4526. https://doi.org/10.1007/s00018-013-1387-

1368   0.

1369 125. Qu, Q., Chen, Y., Wang, Y., Wang, W., Long, S., Yang, H.-Y., Wu, J., Li, M., Tian, X.,

1370   Wei, X., et al. (2024). Lithocholic acid binds TULP3 to activate sirtuins and AMPK to

1371   slow down ageing. Nature. https://doi.org/10.1038/s41586-024-08348-2.

1372 126. Qu, Q., Chen, Y., Wang, Y., Long, S., Wang, W., Yang, H.-Y., Li, M., Tian, X., Wei, X.,

1373   Liu, Y.-H., et al. (2024). Lithocholic acid phenocopies anti-ageing effects of calorie

1374   restriction. Nature. https://doi.org/10.1038/s41586-024-08329-5.

1375 127. Nader, N., Ng, S.S.M., Lambrou, G.I., Pervanidou, P., Wang, Y., Chrousos, G.P., and

1376   Kino, T. (2010). AMPK regulates metabolic actions of glucocorticoids by phosphorylating

1377   the glucocorticoid receptor through p38 MAPK. Mol. Endocrinol. *24*, 1748–1764.

1378   https://doi.org/10.1210/me.2010-0192.

1379 128. Ray, D.W., Suen, C.S., Brass, A., Soden, J., and White, A. (1999). Structure/function of

1380   the human glucocorticoid receptor: Tyrosine 735 is important for transactivation. Mol.

1381   Endocrinol. *13*, 1855–1863. https://doi.org/10.1210/mend.13.11.0376.

1382 129. Sterling, T., and Irwin, J.J. (2015). ZINC 15 – Ligand discovery for everyone. J. Chem.

1383   Inf. Model. *55*, 2324–2337. https://doi.org/10.1021/acs.jcim.5b00559.

1384 130. Knox, C., Wilson, M., Klinger, C.M., Franklin, M., Oler, E., Wilson, A., Pon, A., Cox, J.,

1385   Chin, N.E. (Lucy), Strawbridge, S.A., et al. (2024). DrugBank 6.0: the DrugBank

1386   Knowledgebase for 2024. Nucleic Acids Res. *52*, D1265–D1275.

1387   https://doi.org/10.1093/nar/gkad976.

1388 131. Trott, O., and Olson, A.J. (2010). AutoDock Vina: Improving the speed and accuracy of

1389   docking with a new scoring function, efficient optimization, and multithreading. J.

1390   Comput. Chem. *31*, 455–461. https://doi.org/10.1002/jcc.21334.

1391   132.   Lensink, M.F., Nadzirin, N., Velankar, S., and Wodak, S.J. (2020). Modeling protein-

1392   protein, protein-peptide, and protein-oligosaccharide complexes: CAPRI 7th edition.

1393   Proteins Struct. Funct. Bioinforma. *88*, 916–938. https://doi.org/10.1002/prot.25870.

1394   133.   Jakalian, A., Jack, D.B., and Bayly, C.I. (2002). Fast, efficient generation of high-quality

1395   atomic charges. AM1-BCC model: II. Parameterization and validation. J. Comput. Chem.

1396   *23*, 1623–1641. https://doi.org/10.1002/jcc.10128.

1397   134.   Mazza, D., Abernathy, A., Golob, N., Morisaki, T., and McNally, J.G. (2012). A

1398   benchmark for chromatin binding measurements in live cells. Nucleic Acids Res. *40*,

1399   e119–e119. https://doi.org/10.1093/nar/gks701.

1400   135.   Mikuni, S., Tamura, M., and Kinjo, M. (2007). Analysis of intranuclear binding process of

1401   glucocorticoid receptor using fluorescence correlation spectroscopy. FEBS Lett. *581*, 389–

1402   393. https://doi.org/10.1016/j.febslet.2006.12.038.

1403   136.   Digman, M.A., Dalal, R., Horwitz, A.F., and Gratton, E. (2008). Mapping the number of

1404   molecules and brightness in the laser scanning microscope. Biophys. J. *94*, 2320–2332.

1405   https://doi.org/10.1529/biophysj.107.114645.

1406   137.   Dobin, A., Davis, C.A., Schlesinger, F., Drenkow, J., Zaleski, C., Jha, S., Batut, P.,

1407   Chaisson, M., and Gingeras, T.R. (2013). STAR: ultrafast universal RNA-seq aligner.

1408   Bioinformatics *29*, 15–21. https://doi.org/10.1093/bioinformatics/bts635.

1409   138.   Love, M.I., Huber, W., and Anders, S. (2014). Moderated estimation of fold change and

1410   dispersion for RNA-seq data with DESeq2. Genome Biol. *15*, 550.

1411   https://doi.org/10.1186/s13059-014-0550-8.

1412

Author contributions

1413

1414 Conceptualization: AJP, LV, IA, JFR, PFP, GLH, EEP

1415 Methodology: AJP, TAJ, KW, AAM, IMN, ALL, UE, MS, MA, DMP, DAS

1416 Investigation: AJP, TAJ, KW, AAM, IMN, ALL, UE, MS, MA, DMP, DAS

1417 Visualization: AJP, TAJ, KW, AAM, IMN, IG, ALL, UE, PFP

1418 Funding acquisition: AJP, AAM, JFR, GLH, EEP

1419 Project administration: PFP, GLH, EEP

1420 Supervision: PFP, GLH, EEP

1421 Writing – original draft: AJP, PFP, EEP

1422

Competing interests

1423

1424 Authors declare that they have no competing interests.

1425

Data and materials availability

1426

1427 The Gene Expression profiles are deposited in the Gene Expression Omnibus (GEO) database and

1428 the code assigned is GSE287351. MATLAB-based tracking software is publicly available at

1429 https://doi.org/10.5281/zenodo.7558712. All data reported in this paper will be shared by the lead

1430 contact upon request. Requests for further information or reagents should be directed to and will

1431 be fulfilled by the lead contact, Eva Estébanez-Perpiñá (evaestebanez@ub.edu). No generative AI

1432 or AI-assisted technologies were used at any stage.

1433